J. Fluid Mech. (2008), *vol.* 596, *pp.* 285–311.
doi:10.1017/S0022112007009597 Printed in the United Kingdom

Instability of a viscous coflowing jet in a radial electric field

FANG LI, XIE-YUAN YIN AND XIE-ZHEN YIN

Department of Modern Mechanics, University of Science and Technology of China, Hefei, Anhui 230027, China
xzyin@ustc.edu.cn

(Received 25 June 2006 and in revised form 2 October 2007)

A temporal linear instability analysis of a charged coflowing jet with two immiscible viscous liquids in a radial electric field is carried out for axisymmetric disturbances. According to the magnitude of the liquid viscosity relative to the ambient air viscosity, two generic cases are considered. The analytical dimensionless dispersion relations are derived and solved numerically. Two unstable modes, namely the para-sinuous mode and the para-varicose mode, are identified in the Rayleigh regime. The para-sinuous mode is found to always be dominant in the jet instability. Liquid viscosity clearly stabilizes the growth rates of the unstable modes, but its effect on the cut-off wavenumber is negligible. The radial electric field has a dual effect on the modes, stabilizing them when the electrical Euler number is smaller than a critical value and destabilizing them when it exceeds that value. Moreover, the electrical Euler number and Weber number increase the dominant and cut-off wavenumbers significantly. Based on the Taylor–Melcher leaky dielectric theory, two limit cases, i.e. the small electrical relaxation time limit (SERT) and the large electrical relaxation time limit (LERT), are discussed. For coflowing jets having a highly conducting outer liquid, SERT may serve as a good approximation. In addition, the dispersion relations under the thin layer approximation are derived, and it is concluded that the accuracy of the thin layer approximation is closely related to the values of the dimensionless parameters.

1. Introduction

Coaxial electrospraying is a new effective technique to form micro/nano capsules that are monodisperse and controllable. It has many applications in the drug industry, food additives, paper manufacture, painting and coating processes. In experiments, when two immiscible liquids are emitted from two homocentric capillary tubes, respectively, under appropriate flow and electric field conditions, a stationary Taylor cone is formed. At the tip of the Taylor cone, a steady axisymmetric coaxial jet with nearly uniform diameter arises. The coaxial jet is intrinsically unstable, and breaks up into micro compound droplets at some distance downstream. This is called the cone-jet coaxial electrospraying mode (Loscertales *et al.* 2002).

Recently, many experiments have been carried out to investigate the mechanism of coaxial electrospraying and the scaling laws between important quantities, e.g. Loscertales *et al.* (2002), López-Herrera *et al.* (2003), Chen *et al.* (2005) and Marín *et al.* (2007). Theoretical and numerical work by Li, Yin & Yin (2005, 2006) has analysed the linear instability of an inviscid coaxial jet having a conducting annular liquid under a radial electric field, where both the equipotential and

non-equipotential cases were studied; Higuera (2007) performed a brief but valuable numerical simulation of a stationary electrified coaxial jet in the framework of the leaky dielectric model and quasi-uni-directional approximation.

The breakup process of a liquid jet under an electric field is closely related to the growth and propagation of unstable disturbance waves at the interface between fluids. Therefore, instability analysis is useful in predicting the breakup modes of liquid jets, and also in predicting the intact jet length and droplet size (Chandrasekhar 1961; Shen & Li 1996; Chen & Lin 2002). In the instability analysis of electrically charged single liquid jets, two kinds of electric field, i.e. radial and axial, are usually encountered. Also, the electrical properties of liquids may be of a perfect conductor, perfect dielectric or leaky dielectric (dielectric with finite conductivity). Thus, many cases can arise due to the variation of the electric field imposed on the jet and electrical properties of the liquid. For instance, Turnbull (1992, 1996) analysed the temporal linear stability of conducting and insulating liquid jets in the presence of both radial and axial electric fields; Saville (1971) and Mestel (1994, 1996) studied the stability of a charged leaky dielectric liquid jet under a tangential electric field, paying particular attention to the effect of liquid viscosity; López-Herrera, Riesco-Chueca & Gañán-Calvo (2005) researched the stability of a viscous leaky dielectric liquid jet under a radial electric field, taking into account the effect of ambient air flow. García *et al.* (1997) and González, García & Castellanos (2003) investigated the effect of AC radial electric fields on the instability of liquid jets. Huebner & Chu (1971) and Son & Ohba (1998), respectively, explored the jet instability under axisymmetric and non-axisymmetric disturbances. More recently, nonlinear effects have been specially studied in order to explain the experimental phenomena, such as the formation of satellite droplets (e.g. López-Herrera, Gañán-Calvo & Perez-Saborid 1999; López-Herrera & Gañán-Calvo 2004; Zakaria 2000; Elhefnawy, Agoor & Elcoot 2001; Elhefnawy, Moatimid & Elcoot 2004; Moatimid 2003).

In most of the published reports, the liquid jet is usually assumed to be either perfectly conducting or perfectly dielectric. In practice, most liquids used in experiments are leaky dielectric. Unlike prefect conductors or dielectrics, for leaky dielectrics free charge may occur in the fluid bulk and therefore electromechanical coupling occurs not only at interface but probably also in the bulk. Furthermore, electric stresses on an interface are no longer perpendicular to it, because free charge accumulated on the interface may modify the electric field. From this point of view, electric stresses tangential to the interface are inevitable, and must be balanced by viscous stresses. For perfect conductors or perfect dielectrics, the tangential component of electric stress vanishes, because free charge is reset instantaneously on the interface to keep the interface equipotential for the former, and it is absent for the latter (Saville 1997).

In the authors' previous studies (Li *et al.* 2005, 2006), the assumption that the inner and outer liquids are inviscid was made in the instability analysis of the electrified coaxial jet. However, with such an assumption the tangential component of electric stress on the interface cannot be balanced due to the absence of liquid viscosity. Moreover, liquid viscosity may play an important role in the jet instability, because the diameter of the coaxial jet generated in electrospraying experiments is very small, usually of the order of several tens of micrometres. Therefore, from this physical point of view, it is incorrect to neglect the viscosity of liquid. In the current paper, we propose a viscous leaky dielectric model, based on the theory of the Taylor–Melcher leaky dielectric model (Melcher & Taylor 1969; Saville 1997), to study the axisymmetric instability behaviour of the charged coaxial jet under a radial electric

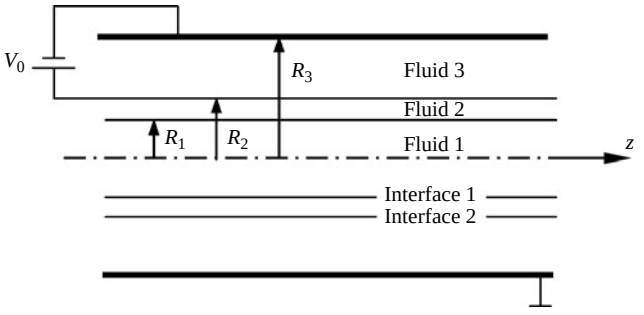

FIGURE 1. Schematic description of the theoretical model.

field. We aim to gain further insight into the outer-driving coaxial electrospraying studied by Li *et al.* (2005, 2006).

Accordingly the outer liquid is assumed to be a leaky dielectric, acting as the driving liquid. Furthermore, the conductivity of the outer liquid is assumed to be large enough so that free charge is relaxed to the interface instantaneously. The inner liquid in the outer-driving coaxial electrospraying, for a generic case, should be considered as a leaky dielectric too. Though the conductivity of the inner fluid is much smaller than that of the outer liquid, it is sufficient to have charge relaxed and transferred to the interface, where the distribution of charge density is determined by the surface charge conservation equation. In such a leaky dielectric case, both the conductivity ratio of inner to outer liquid and the electrical relaxation time of the inner liquid are taken into account. The initial steady state may be solved following the method provided by Higuera (2007). In the outer-driving electrospraying experiments the electrical conductivity of the inner liquid is at least two or three orders of magnitude smaller than that of the outer liquid (López-Herrera *et al.* 2003). Also, in the numerical simulation of Higuera (2007) it was found that the charge density at the inner interface is about two orders smaller than that at the outer interface. Therefore the conductivity of the inner liquid is negligible, and free charge can be supposed to lie approximately only on the outer air–liquid interface in theoretical studies. In our model the inner liquid is approximated as a perfect dielectric and there is no free charge at the inner liquid–liquid interface. Such an approximation can be deduced from the generic leaky dielectric model, assuming that the outer-to-inner conductivity ratio approaches infinite.

The paper is organized as follows. In § 2, the theoretical leaky dielectric model of the viscous coflowing jet is described, and the governing equations and boundary conditions are given. In particular, the basic velocity profile is discussed. The analytical dispersion relation is derived. In § 3, the complex eigenfrequency is calculated numerically. The effects of the viscosity of the inner and outer liquids, the radial electric field and the surface tension are discussed. The cases of small and large electrical relaxation time are outlined. The thin layer approximation is derived and discussed. Finally, the main conclusions are drawn in § 4.

2. Theoretical model

Consider an infinitely long coflowing jet with two immiscible liquids surrounded by the ambient air, as sketched in figure 1. The inner liquid cylinder has a radius R_1, and the outer liquid annulus has an exterior radius R_2. An earthed annular electrode of radius R_3 is positioned surrounding the jet, and a voltage V_0 is imposed

on the jet surface. The electrical property of the outer liquid is assumed to be leaky dielectric; the inner liquid and air are perfect dielectrics. A basic radial electric field of magnitude $-V_0/[r\ln(R_2/R_3)]$ is thus formed in the air. Free charge is assumed to be relaxed on the interface between the air and outer liquid instantaneously, owing to the conductivity of the outer liquid. The density of surface charge on the unperturbed air–liquid interface is $-\varepsilon_3 V_0/[R_2\ln(R_2/R_3)]$.

The liquids and air are considered to be incompressible and Newtonian. The flow is axisymmetric. Effects of gravitational acceleration, magnetic field and temperature are ignored. The governing equations of the flow are

$$\nabla\cdot\boldsymbol{u}_i = 0, \qquad i = 1, 2, 3, \tag{2.1}$$

$$\rho_i\left(\frac{\partial\boldsymbol{u}_i}{\partial t} + \boldsymbol{u}_i\cdot\nabla\boldsymbol{u}_i\right) = -\nabla p_i + \mu_i\nabla^2\boldsymbol{u}_i,\ i = 1, 2, 3, \tag{2.2}$$

where $\boldsymbol{u}$, ρ, p and μ are the velocity, density, pressure and dynamic viscosity, respectively. The subscripts 1, 2 and 3 denote the inner liquid, the outer liquid and the ambient air, respectively.

When the jet is perturbed by an arbitrary disturbance, both the inner liquid–liquid interface and the outer air–liquid interface depart from their original equilibrium positions. For infinitesimal disturbances, their new positions can be expressed as $r = R_j + \eta_j$, $j = 1, 2$, where η_j is the displacement of the interface from R_j, and the subscripts 1 and 2 denote the inner and outer interfaces, respectively. In this paper only the axisymmetric instability is considered, so $\eta_j = \eta_j(z, t)$.

The boundary conditions include the no-slip condition at the electrode, i.e.

$$\boldsymbol{u}_3 = 0 \text{ at } r = R_3; \tag{2.3}$$

the continuity of the velocity at the inner and outer interfaces, i.e.

$$\boldsymbol{u}_2 = \boldsymbol{u}_3 \text{ at } r = R_2 + \eta_2, \tag{2.4}$$

$$\boldsymbol{u}_1 = \boldsymbol{u}_2 \text{ at } r = R_1 + \eta_1; \tag{2.5}$$

the finiteness of the velocity at the symmetric axis, i.e.

$$\boldsymbol{u}_1 < \infty \text{ at } r = 0; \tag{2.6}$$

the kinematic boundary conditions at the interfaces, i.e.

$$u_{1,2} = \left(\frac{\partial}{\partial t} + \boldsymbol{u}_{1,2}\cdot\nabla\right)\eta_1 \text{ at } r = R_1 + \eta_1, \tag{2.7}$$

$$u_{2,3} = \left(\frac{\partial}{\partial t} + \boldsymbol{u}_{2,3}\cdot\nabla\right)\eta_2 \text{ at } r = R_2 + \eta_2, \tag{2.8}$$

where u is the radial velocity component; and the dynamic boundary conditions at the interfaces, i.e.

$$(\boldsymbol{T}_2 - \boldsymbol{T}_1)\cdot\boldsymbol{n}_1 - \gamma_1(\nabla\cdot\boldsymbol{n}_1)\boldsymbol{n}_1 = 0 \text{ at } r = R_1 + \eta_1, \tag{2.9}$$

$$(\boldsymbol{T}_3 - \boldsymbol{T}_2)\cdot\boldsymbol{n}_2 - \gamma_2(\nabla\cdot\boldsymbol{n}_2)\boldsymbol{n}_2 = 0 \text{ at } r = R_2 + \eta_2, \tag{2.10}$$

where $\boldsymbol{T}$ is the stress tensor, γ is the surface tension, $\boldsymbol{n}$ is the normal unit vector and $\nabla\cdot\boldsymbol{n}$ is the curvature. For the axisymmetric case,

$$\boldsymbol{n}_j = \frac{(1, -\eta_{jz})}{\sqrt{1+\eta_{jz}^2}} \text{ and } \nabla\cdot\boldsymbol{n}_j = \frac{1}{\sqrt{1+\eta_{jz}^2}}\left(\frac{1}{R_j+\eta_j} - \frac{\eta_{jzz}}{1+\eta_{jz}^2}\right),\ j = 1, 2,$$

where η_z and η_{zz} are the first- and second-order partial derivatives of η with respect to z, respectively. In the presence of an electric field, the stress tensor $\boldsymbol{T}$ includes not only the hydrodynamic stress tensor but also the electrical Maxwell tensor, i.e. $\boldsymbol{T} = \boldsymbol{T}^h + \boldsymbol{T}^e$, with $\boldsymbol{T}^h = -p\delta + \mu[\nabla \boldsymbol{u} + (\nabla \boldsymbol{u})^T]$ and $\boldsymbol{T}^e = \varepsilon \boldsymbol{E} - \frac{1}{2}\varepsilon \boldsymbol{E} \cdot \boldsymbol{E}\boldsymbol{\delta}$, where $\boldsymbol{\delta}$ is the identity matrix and $\boldsymbol{E}$ is the electric field intensity.

The governing equations and boundary conditions related to the electric field are needed to close the problem. As free charge is absent in the bulk, the Maxwell equations in the liquids and air reduce to

$$\nabla \cdot \boldsymbol{E}_i = 0 \text{ and } \nabla \times \boldsymbol{E}_i = 0, i = 1,\ 2,\ 3.$$

Introduce an electrical potential function ψ_i, satisfying the Laplace equation:

$$\nabla^2 \psi_i = 0, i = 1, 2, 3, \tag{2.11}$$

and the electric field intensity $\boldsymbol{E}_i = -\nabla \psi_i$.

The electrical boundary conditions are (*a*) zero electrical potential at the annular electrode, i.e.

$$\psi_3 = 0 \text{ at } r = R_3; \tag{2.12}$$

(*b*) the finiteness of the electric field at the symmetric axis, i.e.

$$\boldsymbol{E}_1 = 0 \text{ at } r = 0; \tag{2.13}$$

(*c*) continuity of the tangential component of the electric field at the inner and outer interfaces, i.e.

$$n_j \times [E] = 0 \text{ at } r = R_j + \eta_j,\ j = 1, 2, \tag{2.14}$$

where the symbol $[\cdot]$ indicates the jump of the corresponding quantity across the interface; (*d*) continuity of the normal component of the electric displacement at the inner interface, i.e.

$$n_1 \cdot (\varepsilon_2 E_2 - \varepsilon_1 E_1) = 0 \text{ at } \quad r = R_1 + \eta_1; \tag{2.15}$$

and (*e*) the Gauss law at the outer interface, i.e.

$$n_2 \cdot (\varepsilon_3 E_3 - \varepsilon_2 E_2) = q_s \text{ at } r = R_2 + \eta_2, \tag{2.16}$$

where the surface charge density q_s satisfies the surface charge conservation equation

$$\frac{\partial q_s}{\partial t} + \boldsymbol{u} \cdot \nabla q_s - q_s \boldsymbol{n} \cdot (\boldsymbol{n} \cdot \nabla)\boldsymbol{u} + [\sigma \boldsymbol{E}] \cdot \boldsymbol{n} = 0. \tag{2.17}$$

The four terms on the left-hand side of equation (2.17) represent the contributions of charge accumulation, surface convection, surface dilation and bulk conduction, respectively (Saville 1997).

Before the instability analysis, the basic velocity profile of the jet in the unperturbed state should be obtained. As the jet is perfectly cylindrical and the flow is axisymmetric, the basic velocity field is unidirectional, i.e. $\boldsymbol{u} = W(r)\boldsymbol{e}_z$, where W is the axial velocity component and $\boldsymbol{e}_z$ is the unit vector in the axial direction. Therefore the momentum equation (2.2) reduces to

$$\left(\frac{\mathrm{d}^2 W_i}{\mathrm{d}r^2} + \frac{1}{r}\frac{\mathrm{d}W_i}{\mathrm{d}r}\right) = -\frac{G_i}{\mu_i}, i = 1, 2, 3, \tag{2.18}$$

where $G_i = -\partial p_i / \partial z$ is the negative of the streamwise pressure gradient (Chen & Lin 2002). According to the balance of forces on the interfaces, the pressure gradients in the liquids and air should be equal, i.e. $G_i = G$. Integrating (2.18) and using the

continuity conditions of the velocity and shear force on the interfaces, the solutions of W_i are obtained. Choosing μ_2, R_2, and U_2 (the velocity of the jet at the outer interface, $= G(R_3^2 - R_2^2)/(4\mu_3)$) as the scales of dynamic viscosity, length and velocity, respectively, we write the solutions W_i in the following dimensionless form:

$$W_3 = \frac{b^2 - r^2}{b^2 - 1}, \tag{2.19a}$$

$$W_2 = 1 + \mu_{r3}\frac{1 - r^2}{b^2 - 1}, \tag{2.19b}$$

$$W_1 = 1 + \mu_{r3}\frac{1 - a^2}{b^2 - 1} + \frac{\mu_{r3}}{\mu_{r1}}\frac{a^2 - r^2}{b^2 - 1}, \tag{2.19c}$$

where two radius ratios are $a = R_1/R_2$, $b = R_3/R_2$, and two viscosity ratios are $\mu_{r1} = \mu_1/\mu_2$, $\mu_{r3} = \mu_3/\mu_2$. Note that the logarithm function $\ln r$ included in general solution of equation (2.18) by Chen & Lin (2002) vanishes owing to the absence of the gravitational acceleration.

It can be seen from equations (2.19*a*)–(2.19*c*) that the basic velocity profile is closely associated with the relative viscosity of the inner liquid and outer liquid and that of air and the outer liquid. First, suppose the ambient air is almost inviscid, i.e. $\mu_{r3} \ll 1$. According to equation (2.19*b*) the basic axial velocity of the outer liquid is nearly uniform, i.e. $W_2 \simeq 1$. For the inner liquid, there are two cases: if its viscosity is of the order of the air viscosity (i.e. $\mu_{r1} \sim O(\mu_{r3})$), such as a dense gas (without lose of generality, the inner liquid can be gas.), it can be seen from equation (2.19*c*) that the corresponding basic velocity profile is still parabolic; conversely, if its viscosity is much larger than that of the air (i.e. $\mu_{r1} \gg \mu_{r3}$), such as various polymers and oils, the basic velocity profile is also approximately uniform with the same magnitude as the outer liquid. Therefore, in general, according to the magnitude of the inner liquid viscosity, two cases are involved.

Case I: $\mu_{r1} \sim O(\mu_{r3})$, the basic axial velocity profile is

$$W_3 = 1 + \frac{1 - r^2}{b^2 - 1}, \quad W_2 \simeq 1, \quad W_1 \simeq 1 + \boldsymbol{\Lambda}\left(1 - \frac{r^2}{a^2}\right), \tag{2.20}$$

where the relative velocity ratio $\boldsymbol{\Lambda} = U_0/U_2 - 1$ (U_0 is the velocity of the jet at the symmetric axis $r = 0$, $\simeq 1 + (\mu_{r3}/\mu_{r1})(a^2/(b^2 - 1))$. Case II: $\mu_{r1} \gg \mu_{r3}$, the basic velocity profile is

$$W_3 = 1 + \frac{1 - r^2}{b^2 - 1}, \quad W_2 \simeq 1, \quad W_1 \simeq 1. \tag{2.21}$$

Figure 2 shows two typical basic velocity profiles; the axial velocity profile of the inner liquid is apparently parabolic for $\mu_{r1} = 0.018$, corresponding to case I, and appears to be uniform for $\mu_{r1} = 43$, corresponding to case II. In the following instability analysis we assume that the outer liquid is viscous and the air is inviscid in both cases and that the inner liquid is inviscid in case I and is viscous in case II. The advantage of this is that an analytical dispersion relation can be obtained. Moreover, the continuity of tangential force seems to be satisfied inherently for the simplified velocity profiles in both cases. Numerical studies of the instability of a viscous coaxial jet with leaky dielectric liquids in a radial electric field, have to our knowledge not be reported before. The purpose of the present paper is to study this complicated problem using a simplified theoretical model.

If an axisymmetric jet of a viscous liquid is subjected to an axial electric field, its basic axial velocity profile is essentially parabolic, owing to the action of electrical

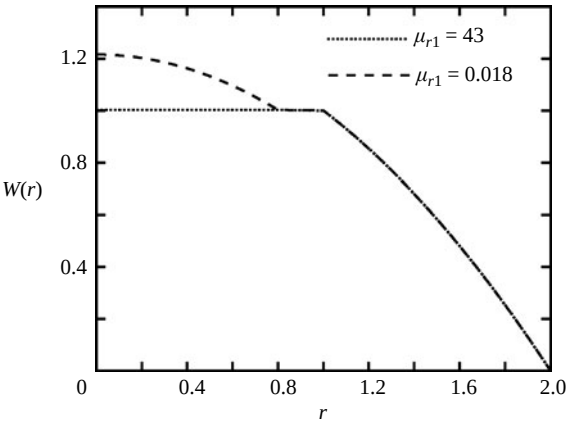

FIGURE 2. The influence of the relative viscosity of the inner liquid on the basic velocity profile, for $\mu_{r3} = 0.018$, $a = 0.8$ and $b = 2$.

shear stress (Mestel 1994, 1996). However, as is well known, if both the viscosity and the non-uniform velocity profile are considered, the dispersion relation in an analytical form is beyond reach. In such a case either the velocity profile is assumed to be uniform (Saville 1971; López-Herrera *et al.* 2005), or the viscosity of the liquid is assumed to be low or high (Mestel 1994, 1996), or the wavelength of the disturbance is assumed to be long (Turnbull 1992, 1996). But in this paper a radial electric field not an axial electric field is studied. In the presence of a radial electric field the electrical shear stress in the unperturbed state is absent as discussed above, and so the basic velocity profile for viscous liquids can reasonably be considered to be uniform.

The Froude number $Fr = U^2/gL$ (U is the characteristic velocity; g is the gravitational acceleration; L the characteristic length) measures the relative effect of gravity. If the characteristic length of the coaxial jet is not so small, Fr is finite. In such a case, gravity may be as important as the axial electric field. Both gravity and the axial electric field induce non-uniformity of the basic axial velocity, but their effects may be opposite: if the axial electric field is in the same direction as gravity (which is in accordance with most experimental situations), the electrical shear force makes the velocity at the interface larger than in the liquid bulk, and with the spatial evolution of the jet its effect is diffused into the bulk owing to liquid viscosity; on the other hand, gravity, acting as a pressure gradient, induces a larger velocity in the liquid centre. Consequently, the action of the axial electric field and gravity may reach an equilibrium state as the jet evolves spatially and the well-developed jet has an axial uniform velocity. In such a case, the uniform velocity profile approximation is appropriate.

For infinitesimal axisymmetric disturbances, the perturbation of the interface (and also of the other physical quantities), is decomposed into the form of a Fourier exponential, i.e. $\eta_j(z, t) = \hat{\eta}_j \exp(\omega t + \mathrm{i}kz)$, j=1, 2, where $\hat{\eta}_j$ is the initial amplitude of the perturbation at the interface, ω is the complex wave frequency, the real and imaginary parts of which are the temporal growth rate and frequency, respectively, k is the real axial wavenumber related to the wavelength by $k = 2\pi/\lambda$, and the imaginary unit $\mathrm{i} = \sqrt{-1}$. Substituting the perturbation expression into the governing equations and boundary conditions (2.1)–(2.17), the dispersion relation between ω and k is obtained. The derivation details are given in Appendix A.

Choosing ρ_2, γ_2, $\rho_2 U_2^2$, ε_3 and $-V_0/[R_2\ln(R_2/R_3)]$ as the characteristic scales of density, surface tension, pressure, electrical permittivity and electric field intensity, respectively, the dispersion relation is written in the following dimensionless form:

$$D(k,\omega)=\left(\frac{\hat{\eta}_2}{\hat{\eta}_1}\right)_1\left(\frac{\hat{\eta}_1}{\hat{\eta}_2}\right)_2-1=0, \tag{2.22}$$

for case I, where $(\hat{\eta}_2/\hat{\eta}_1)_1$ and $(\hat{\eta}_1/\hat{\eta}_2)_2$ are the amplitude ratio of the initial disturbances at the interfaces, expressed as

$$\begin{aligned}\left(\frac{\hat{\eta}_2}{\hat{\eta}_1}\right)_1=&\left[\frac{l^2+k^2}{a}\Delta_4\left(\frac{EuRe\zeta}{\omega}+1+\frac{l^2}{k^2}\right)-\frac{2k^2}{a}\Delta_3\left(\frac{EuRe\zeta}{\omega}+2\right)\right]^{-1}\\&\times\left[Re^2H_1\Delta_3\Delta_4-4lk^2\Delta_3\left(\Delta_6-\frac{1}{la}\Delta_4\right)+\Delta_4\left((l^2+k^2)\Delta_1-\frac{2k}{a}\Delta_3\right)\frac{l^2+k^2}{k}\right.\\&\left.+\left(\frac{2k^2}{a}\Delta_3-\frac{l^2+k^2}{a}\Delta_4\right)\frac{EuRe\xi}{\omega}\right]\end{aligned} \tag{2.23a}$$

and

$$\begin{aligned}\left(\frac{\hat{\eta}_1}{\hat{\eta}_2}\right)_2=&\left[4k^2\Delta_3-\frac{(l^2+k^2)^2}{k^2}\Delta_4+k((l^2+k^2)\Delta_2\Delta_4-2lk\Delta_3\Delta_5)\frac{EuRe\xi}{\omega}\right.\\&\left.-Re^2\Delta_3\Delta_4Euk\xi J\right]^{-1}\left[Re^2H_2\Delta_3\Delta_4-k\Delta_4((l^2+k^2)\Delta_2\right.\\&\left.+2k\Delta_3)\left(\frac{EuRe\zeta}{\omega}+1+\frac{l^2}{k^2}\right)+2lk^2\Delta_3\left(\Delta_5+\frac{1}{l}\Delta_4\right)\left(\frac{EuRe\zeta}{\omega}+2\right)\right],\end{aligned} \tag{2.23b}$$

respectively. The amplitude ratio $(\hat{\eta}_2/\hat{\eta}_1)_1$ comes mainly from the dynamic balance at the inner interface and $(\hat{\eta}_1/\hat{\eta}_2)_2$ from the dynamic balance at the outer interface. The symbols appearing in the dispersion equation are

$$H_1=\frac{\mathrm{i}S\omega}{k}\left(\mathrm{i}\omega\frac{I_0(ka)}{I_1(ka)}-\frac{2\Lambda}{a}\right)+\frac{\Gamma}{We\,a^2}(1-(ka)^2), \tag{2.24a}$$

$$H_2=\frac{\mathrm{i}Q\omega}{k}\left(\mathrm{i}\omega L-\frac{2}{b^2-1}\right)+Eu(1+k(\zeta+1)J)-\frac{1}{We}(1-k^2), \tag{2.24b}$$

$$J=\frac{I_1(k)K_0(kb)+K_1(k)I_0(kb)}{I_0(k)K_0(kb)-K_0(k)I_0(kb)}, \tag{2.24c}$$

$$\zeta=\frac{-k\left(1+\dfrac{l^2}{k^2}\right)\dfrac{\Delta_2}{\Delta_3}+2l\dfrac{\Delta_5}{\Delta_4}+\dfrac{Re\omega J}{k}}{\dfrac{Re}{k}(\varepsilon_{r2}(\omega+\tau)\kappa-\omega J)+\dfrac{EuRe}{\omega}\left(k\dfrac{\Delta_2}{\Delta_3}-l\dfrac{\Delta_5}{\Delta_4}\right)}, \tag{2.24d}$$

$$\xi=\frac{\left(1+\dfrac{l^2}{k^2}\right)\dfrac{1}{\Delta_3}-\dfrac{2}{\Delta_4}}{\dfrac{Re}{k}(\varepsilon_{r2}(\omega+\tau)\kappa-\omega J)+\dfrac{EuRe}{\omega}\left(k\dfrac{\Delta_2}{\Delta_3}-l\dfrac{\Delta_5}{\Delta_4}\right)}, \tag{2.24e}$$

with

$$L = \frac{I_0(k)K_1(kb) + K_0(k)I_1(kb)}{I_1(k)K_1(kb) - K_1(k)I_1(kb)}, \quad \kappa = -\frac{I_1(ka)\Delta_1 - \dfrac{\varepsilon_{r2}}{\varepsilon_{r1}}I_0(ka)\Delta_3}{I_1(ka)\Delta_0 - \dfrac{\varepsilon_{r2}}{\varepsilon_{r1}}I_0(ka)\Delta_2}.$$

And $\Delta_0 - \Delta_6$ are

$$\Delta_0 = I_0(ka)K_0(k) - K_0(ka)I_0(k), \quad \Delta_1 = I_0(ka)K_1(k) + K_0(ka)I_1(k),$$
$$\Delta_2 = I_1(ka)K_0(k) + K_1(ka)I_0(k), \quad \Delta_3 = I_1(ka)K_1(k) - K_1(ka)I_1(k),$$
$$\Delta_4 = I_1(la)K_1(l) - K_1(la)I_1(l), \quad \Delta_5 = I_1(la)K_0(l) + K_1(la)I_0(l),$$
$$\Delta_6 = I_0(la)K_1(l) + K_0(la)I_1(l),$$

where $I_n(x)$ and $K_n(x)$ ($n = 0, 1$) are the nth-order modified Bessel functions of the first and second kinds. Here the wavenumber k and complex frequency ω have been normalized by $1/R_2$ and U_2/R_2, respectively. In the following numerical section, we mainly take case I as an example to illuminate the unstable modes and behaviours of a viscous coflowing jet under a radial electric field. Case II is calculated when studying the effect of the inner liquid viscosity and in part of the thin layer approximation. The dispersion relation for case II is given in Appendix B.

The dimensionless parameters involved in the dispersion relation (2.22) include
the density ratios $S = \rho_1/\rho_2$ and $Q = \rho_3/\rho_2$,
the interfacial tension coefficient ratio $\Gamma = \gamma_1/\gamma_2$,
the electrical permittivity ratios $\varepsilon_{r1} = \varepsilon_1/\varepsilon_3$ and $\varepsilon_{r2} = \varepsilon_2/\varepsilon_3$,
the relative electrical relaxation time $\tau = R_2\sigma_2/U_2\varepsilon_2$,
the Reynolds number $Re = \rho_2 U_2 R_2/\mu_2$,
the Weber number $We = \rho_2 U_2^2 R_2/\gamma_2$,
the electrical Euler number $Eu = \varepsilon_3 V_0^2/\rho_2 U_2^2 R_2^2 \ln^2(R_2/R_3)$.
The last three dimensionless parameters represent the relative magnitudes of the viscous force, surface tension and electrical force to the inertia force, respectively.

In most experiments, R_3 is much larger than R_2, i.e. the radius ratio $b \gg 1$. In the dispersion relation (2.22) the parameter b appears only in J and L, for which we have the limits:

$$J|_{b\to\infty} = -K_1(k)/K_0(k) \text{ and } L|_{b\to\infty} = -K_0(k)/K_1(k).$$

For large Reynolds numbers ($Re \gg 1$), the dispersion relation (2.22) and the amplitude ratios (2.23a, b) can be simplified dramatically to

$$D(k, \omega) = ak^2(T_1\Delta_3 - \Delta_1)(T_2\Delta_3 + \Delta_2) + 1 = 0, \tag{2.25}$$

and

$$\left(\frac{\hat{\eta}_2}{\hat{\eta}_1}\right)_1 = -ak(T_1\Delta_3 - \Delta_1), \left(\frac{\hat{\eta}_1}{\hat{\eta}_2}\right)_2 = k(T_2\Delta_3 + \Delta_2), \tag{2.26}$$

with

$$T_1 = -\omega^{-2}\left[\frac{\mathrm{i}S\omega}{k}\left(\mathrm{i}\omega\frac{I_0(ka)}{I_1(ka)} - \frac{2\Lambda}{a}\right) + \frac{\Gamma}{We\,a^2}(1 - (ka)^2)\right],$$
$$T_2 = \omega^{-2}\left[\mathrm{i}Q\omega\left(-\mathrm{i}\omega L + \frac{2}{b^2 - 1}\right) - Euk(1 + kJ) + \frac{k}{We}(1 - k^2)\right].$$

If the relative velocity ratio $\Lambda = 0$, the dispersion relation (2.25) is consistent with that for the electrified coaxial jet in the equipotential case where Λ is fixed to 1 (Li *et al.* 2005).

In addition, the dispersion relation (2.22) can be reduced to that for a single-liquid jet in a simple way. If the radius ratio a approaches zero, the jet consists only of the outer leaky dielectric liquid. The inner interface vanishes, and the numerator of (2.23b) is zero, yielding

$$Re^2 H_2 - k\left((l^2+k^2)\frac{\Delta_2}{\Delta_3}+2k\right)\left(\frac{EuRe\zeta}{\omega}+1+\frac{l^2}{k^2}\right) + 2lk^2\left(\frac{\Delta_5}{\Delta_4}+\frac{1}{l}\right)\left(\frac{EuRe\zeta}{\omega}+2\right)=0, \quad (2.27)$$

where $\Delta_2/\Delta_3 = -I_0(k)/I_1(k)$, $\Delta_5/\Delta_4 = -I_0(l)/I_1(l)$ and

$$\zeta = \frac{k\dfrac{I_0(k)}{I_1(k)}\left(1+\dfrac{l^2}{k^2}\right)-2l\dfrac{I_0(l)}{I_1(l)}+\dfrac{Re\omega J}{k}}{\dfrac{Re}{k}\left(\varepsilon_{r2}(\omega+\tau)\kappa-\omega J\right)+\dfrac{EuRe}{\omega}\left(-k\dfrac{I_0(k)}{I_1(k)}+l\dfrac{I_0(l)}{I_1(l)}\right)}.$$

After some algebra, the above equation is written in a clearer form:

$$\varsigma\omega^2+\frac{2\omega}{Re}(2k^2\varsigma-1)+\frac{4k^2}{Re^2}(k^2\varsigma-l^2\varsigma_v)+T+\left(1+\frac{Euk\varsigma}{EJ\omega^2}(l^2\varsigma_v-k^2\varsigma)\right)^{-1} \left[\frac{2Eu\varsigma k^2}{EJRe\omega}\left(2+\frac{1}{kJ}\right)(k^2\varsigma-l^2\varsigma_v)+\frac{Eu\varsigma}{E}\left(2k^2\varsigma+\frac{k\varsigma l^2\varsigma_v}{J}+kJ\right)\right]=0, \quad (2.28)$$

where

$$\varsigma(k)=\frac{I_0(k)}{kI_1(k)}, \quad \varsigma_v(l)=\frac{I_0(l)}{lI_1(l)},$$

$$E=\frac{\varepsilon_{r2}}{kJ}\left(1+\frac{\tau}{\omega}\right)-\varsigma, \quad T=\frac{iQ\omega}{k}\left(i\omega L-\frac{2}{b^2-1}\right)+Eu(1+kJ)-\frac{1}{We}(1-k^2).$$

Equation (2.28) is the dispersion relation for a viscous jet with a leaky dielectric liquid, which exactly corresponds with López-Herrera *et al.* (2005).

3. Numerical results

The dimensionless dispersion relation (2.22) is a quartic equation for the complex frequency ω. Given an axial wavenumber k, there are generally four eigenvalues corresponding to four different modes, but only two of the modes are unstable in the Rayleigh regime (Chen & Lin 2002); these are usually called the para-sinuous mode and the para-varicose mode. Suppose the interface perturbation amplitude ratio $\hat{\eta}_1/\hat{\eta}_2 = |\hat{\eta}_1/\hat{\eta}_2|\exp(\mathrm{i}(\theta_1-\theta_2))$, where $|\hat{\eta}_1/\hat{\eta}_2|$ is the relative magnitude of the amplitudes, and $\Delta\theta = \theta_1-\theta_2$ is the corresponding phase difference. The para-sinuous mode means that the inner liquid–liquid interface and the outer air–liquid interface are perturbed almost in phase, i.e. $\Delta\theta$ approaches 0°; and the para-varicose mode means that the two interfaces are perturbed nearly out of phase, i.e. $\Delta\theta$ approaches 180°. Under most experimental situations (López-Herrera *et al.* 2003), the para-sinuous mode is less stable than the para-varicose one and is dominant in the jet instability, promoting the formation of compound droplets. However, as long as the unstable para-varicose mode exists, coaxial electrospraying is negatively influenced by it. On the other hand, under a sufficiently intense electric field and sufficiently large flow rate, those non-axisymmetric modes may become comparable to the axisymmetric

ones, and even become dominant (Son & Ohba 1998; Li *et al.* 2005, 2006). In the present paper we study the theoretical model for the axisymmetric instability, and try to maintain the axisymmetric modes dominant through controlling the values of the dimensionless parameters. The non-axisymmetric instability deserves special study.

In this section, we solve (2.22) numerically in order to study the behaviour of the coaxial jet under the radial electric field, mainly taking case I as an example. For convenience of calculation and comparison, a set of dimensionless parameters is chosen as a reference set. In case I, we take water and air as the outer and inner liquids, respectively, because water is the most common leaky dielectric and air is a common perfect dielectric, corresponding to the case of the outer-driving coaxial electrospraying studied in the paper. Their physical properties can be found in López-Herrera *et al.* (2003). The reference dimensionless parameters are $Q = 0.001$, $S = 0.001$, $a = 0.8$, $b = 10$, $\Lambda = 0.2$, $Re = 10$, $We = 10$, $\Gamma = 1$, $Eu = 0.15$, $\varepsilon_{r1} = 1$, $\varepsilon_{r2} = 80$ and $\tau = 1$. In the calculation the dimensionless parameters are fixed to the reference values unless stated otherwise.

3.1. *Effect of liquid viscosity and comparison with the inviscid model*

In order to study the effect of the viscosity of the outer liquid, we first establish an inviscid model. In the inviscid model, both the inner liquid and the outer liquid are assumed to be inviscid, and the velocities of the inner and outer liquids in the basic state are assumed to be uniform with a discontinuity at the inner and outer interfaces. Denoting the base axial velocities of the inner and outer liquids by U_1 and U_2, respectively, a new dimensionless parameter $\Lambda^\dagger = U_1/U_2 - 1$ is obtained. For leaky dielectrics, the dimensionless dispersion relation of this inviscid model is also expressed in the form of equation (2.22), but with different perturbation amplitude ratios:

$$\left(\frac{\hat{\eta}_2}{\hat{\eta}_1}\right)_1 = \frac{k^2 a H_1 \Delta_3 + ka\omega^2 \Delta_1}{\omega^2}, \tag{3.1a}$$

$$\left(\frac{\hat{\eta}_1}{\hat{\eta}_2}\right)_2 = -\frac{k^2 H_2 \Delta_3 - k\omega^2 \Delta_2}{\omega^2 + Euk^3 J\xi \Delta_3}, \tag{3.1b}$$

where

$$H_1 = -\frac{S(\omega + i\Lambda^\dagger k)^2 I_0(ka)}{kI_1(ka)} + \frac{\Gamma}{We\, a^2}(1 - (ka)^2), \tag{3.2a}$$

$$H_2 = -\frac{Q\omega^2}{k} L + Eu(1 + k(\zeta + 1)J) - \frac{1}{We}(1 - k^2), \tag{3.2b}$$

$$\zeta = \frac{k\omega(J - \Delta_2/\Delta_3)}{k\varepsilon_{r2}(\omega + \tau)\kappa - k\omega J}, \tag{3.2c}$$

$$\xi = \frac{\omega/\Delta_3}{k\varepsilon_{r2}(\omega + \tau)\kappa - k\omega J}. \tag{3.2d}$$

The other symbols are the same as in the viscous model. The coordinate system in this inviscid model is still moving with velocity U_2.

Note that the dispersion relation for the inviscid model is a little different from equation (2.25) for the case of large Reynolds numbers, because the tangential dynamic continuity condition at the outer interface is treated differently in these two cases. In the large-Re case the tangential component of the electrical stress at the outer interface is very small, or even vanishes. In such a case the jet surface can be

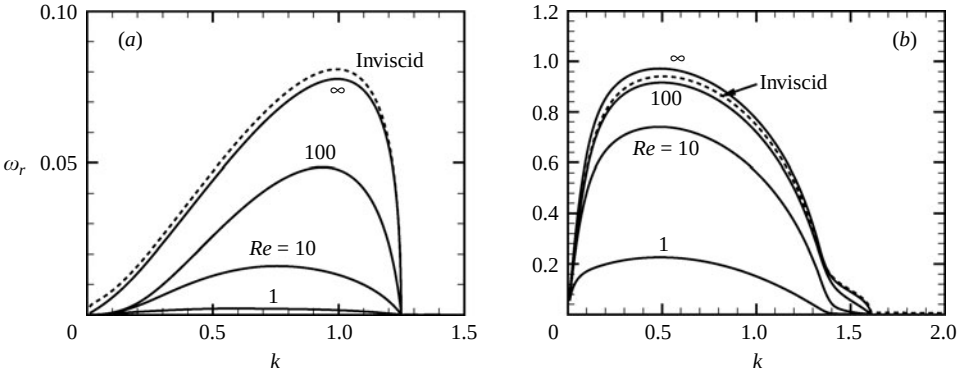

FIGURE 3. The influence of the Reynolds number on the growth rates of (*a*) the para-varicose mode and (*b*) the para-sinuous mode, for $\Lambda = 0$. The dashed curves are for the inviscid leaky dielectric model.

regarded to be approximately equipotential. However, in the inviscid leaky dielectric case, the tangential dynamic condition is not satisfied because the viscous shear is not taken into account, and the jet may be non-equipotential. The dispersion relation given by (3.1*a*, *b*) reduces to that for the equipotential case only if the relative electrical relaxation time τ approaches infinity (Li *et al.* 2005). In addition, if τ approaches zero it is reduced to the dispersion relation for the non-equipotential case (Li *et al.* 2006).

The influence of the viscosity of the outer liquid on the unstable modes is shown in figure 3, where the relative velocity ratio $\Lambda = 0$. For comparison, the curves for the large Reynolds number limit (marked with '∞') and the inviscid leaky dielectric model with the relative velocity ratio $\Lambda^{\dagger} = 0$ (dashed) are also plotted. It is clear that the growth rates of both the para-varicose mode in figure 3(*a*) and the para-sinuous mode in figure 3(*b*) are greatly enhanced as the Reynolds number increases, indicating that the viscosity of the outer liquid has a remarkable stabilizing effect on the jet instability. For the para-sinuous mode, the large-R_e limit, i.e. the equipotential case, is the most unstable. However, for the para-varicose mode, the inviscid leaky dielectric model possesses the maximum growth rate. In general these two special cases are very close. The reason may be that the reference value of the relative electrical permittivity of the outer liquid is so high ($\varepsilon_{r2} = 80$) that the denominators of (3.2*c*) and (3.2*d*) are large enough to make the effects of ζ and ξ negligible. On the other hand, it is shown in the figure that the viscosity of the outer liquid has no apparent effect on the range of the unstable axial wavenumbers. The cut-off wavenumber k_c is approximately 1.25 for the para-varicose mode and 1.6 for the para-sinuous mode.

In case I, the basic velocity profile of the inner liquid is parabolic, as defined in equation (2.20), where a dimensionless parameter Λ is involved. Apparently, this parameter represents the effect of the shear in the axial velocity on the jet instability. The influence of Λ on the growth rates of the unstable modes is illustrated in figure 4. As the density ratio S (=0.001) in the reference state is so small that the effect of Λ cannot be shown clearly, in the calculation the value of S is chosen to be 0.1. Although the density ratio S is increased, the para-varicose mode is little influenced, as shown in figure 4(*a*). In figure 4(*b*) the para-sinuous mode is stabilized slightly as Λ increases. If the density of the inner liquid is comparable to that of the outer liquid, the effect of Λ becomes more significant. The calculation shows that the growth rate of the para-varicose mode is also reduced as Λ increases. It is well known that the

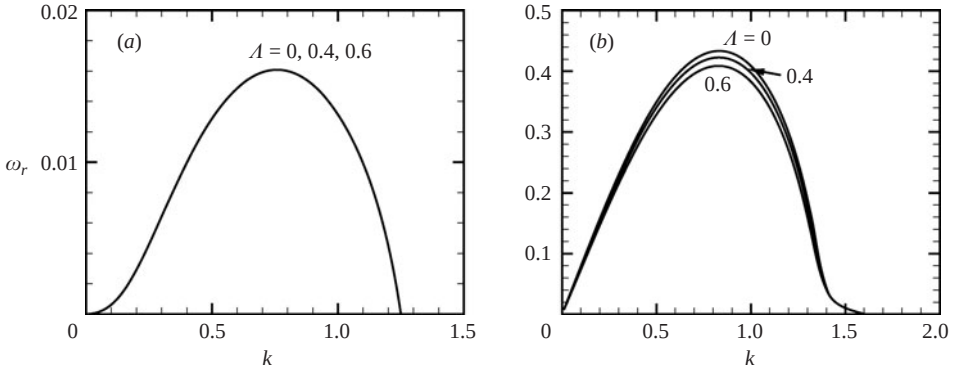

FIGURE 4. The influence of the relative velocity ratio Λ on the growth rates of (*a*) the para-varicose mode and (*b*) the para-sinuous mode, for $S = 0.1$.

para-sinuous and para-varicose modes are associated primarily with the inner and outer interfaces (Chen & Lin 2002; Li *et al.* 2005, 2006), respectively. Apparently, the parameter Λ influences the mode closely connected with the inner interface more strongly. In general, our result is in accordance with the fact that the shear in the axial velocity has a stabilizing effect on the jet instability (Mestel 1994). Similar to the liquid viscosity, the shear in the axial velocity has a negligible effect on the unstable wavenumber range. The critical wavenumber is approximately the same as shown in figure 3.

In coaxial electrospraying experiments with two liquids, the inner one is usually highly viscous (López-Herrera *et al.* 2003; Chen *et al.* 2005). However, in case I the viscosity of the inner liquid is neglected. Therefore, it is necessary to study the jet instability in case II, in which the inner liquid viscosity is allowed to be comparable to or larger than that of the outer liquid. We take sunflower oil as the inner dielectric liquid. Its physical properties can be found in López-Herrera *et al.* (2003). Figure 5 illustrates the effect of the relative viscosity of the inner liquid $\mu_r = \mu_1/\mu_2$ on the growth rates of the unstable modes, where the other parameters are $Q = 0.001$, $S = 0.84$, $a = 0.8$, $b = 10$, $\Lambda = 0.2$, $Re = 10$, $We = 10$, $\Gamma = 0.23$, $Eu = 0.15$, $\varepsilon_{r1} = 3.4$, $\varepsilon_{r2} = 80$ and $\tau = 1$. In the figure, both the para-varicose and para-sinuous modes are stabilized greatly by the viscosity of the inner liquid. In particular, for relatively large viscosity ratio μ_r the growth rates of both the modes are much smaller than in the inviscid case $\mu_r = 0$, indicating that the jet goes a long way before breakup. Like the viscosity of the outer liquid, the inner liquid viscosity has a negligible effect on the range of the unstable wavenumbers.

3.2. *Discussion on the electrical relaxation time and two limiting cases*

For EHD leaky dielectrics, there are two important characteristic times, i.e. the electrical relaxation time and the hydrodynamic time. The electrical relaxation time $\tau_e \sim \varepsilon/\sigma$ measures the speed of charge relaxation, i.e. the contribution of conduction to charge transportation. The hydrodynamic time can have several definitions, such as the capillary time $\tau_c \sim (\rho L^3/\gamma)^{1/2}$, the viscous diffusion time $\tau_v \sim \rho L^2/\mu$, and the convective flow time $\tau_F \sim L/U$. In this model, we choose the convective flow time $\tau_F \sim R_2/U_2$ as the characteristic hydrodynamic time, which measures the contribution of convection to charge transportation. As a result, a dimensionless parameter $\tau = (R_2\sigma_2)/(U_2\varepsilon_2)$ measuring the relative magnitude of the hydrodynamic

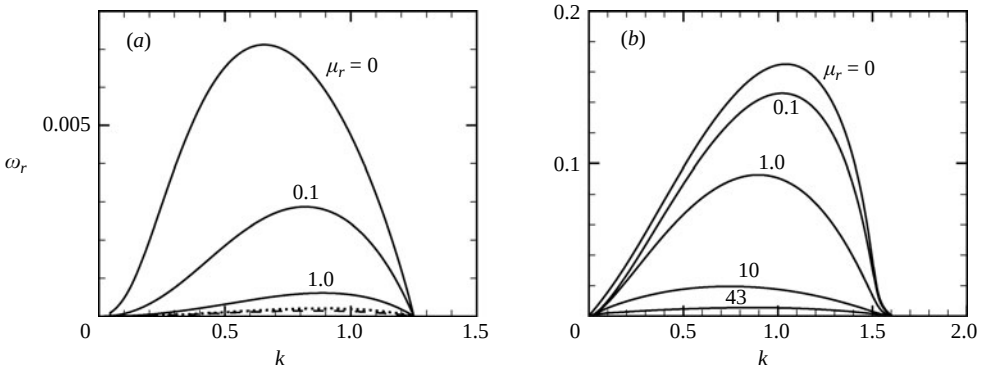

FIGURE 5. The influence of the relative viscosity of the inner liquid on the growth rates of (*a*) the para-varicose mode and (*b*) the para-sinuous mode. The other parameters are $Q = 0.001$, $S = 0.84$, $a = 0.8$, $b = 10$, $\Lambda = 0.2$, $Re = 10$, $We = 10$, $\Gamma = 0.23$, $Eu = 0.15$, $\varepsilon_{r1} = 3.4$, $\varepsilon_{r2} = 80$ and $\tau = 1$. The dotted and dashed curves in (*a*) are for $\mu_r = 10$ and 43, respectively.

time and the electrical relaxation time, i.e. the relative importance of conduction and convection, is involved in the dispersion relation (2.22).

In this section, we derive two limiting cases according to the relative magnitude of the electrical relaxation time and the hydrodynamic time in a more generic sense. Selecting an appropriate hydrodynamic time τ_h, the surface charge conservation equation (2.17) is non-dimensionalized as follows:

$$\frac{\partial q_s}{\partial t} + \boldsymbol{u}\cdot\nabla q_s - q_s\boldsymbol{n}\cdot(\boldsymbol{n}\cdot\nabla)\boldsymbol{u} + \frac{\tau_h}{\tau_e}[\sigma\boldsymbol{E}]\cdot\boldsymbol{n} = 0. \tag{3.3}$$

For well-conducting liquids, the electrical relaxation time τ_e is usually several orders of magnitude smaller than the hydrodynamic time τ_h, i.e. $\tau_h \gg \tau_e$, indicating that charge is transported mainly by conduction and the effect of convection is negligible. This case is called the small electrical relaxation time limit (SERT). In this limit the surface charge conservation equation (3.3) reduces to

$$[\sigma\boldsymbol{E}]\cdot\boldsymbol{n} = 0. \tag{3.4}$$

Note that the surface charge density is absent in equation (3.4). It can be obtained through the boundary condition (2.16). In our model, the condition (3.4), which is obeyed at the outer air–liquid interface, implies that the outer liquid is equipotential (i.e. the equipotential case).

Conversely, for relatively imperfectly conducting liquids with a relatively high velocity, the electric relaxation time τ_e may be much larger than the hydrodynamic time τ_h, i.e. $\tau_h \ll \tau_e$. In such a case charge convection becomes significant and the effect of conduction is negligible. It is called the large electrical relaxation time limit (LERT). In this limit equation (3.3) reduces to

$$\frac{\partial q_s}{\partial t} + \boldsymbol{u}_s\cdot\nabla q_s - q_s\boldsymbol{n}_s\cdot(\boldsymbol{n}_s\cdot\nabla)\boldsymbol{u}_s = 0, \tag{3.5}$$

where only the bulk conduction disappears, corresponding to the non-equipotential case. In case LERT, charge at the interface cannot be reset instantaneously to maintain the interface equipotential. Equation (3.5) may serve as the surface charge conservation equation for this limit. In the study of the interfacial instability of a conducting liquid jet under a radial electric field (Artana, Romat & Touchard 1998;

Li *et al.* 2006), both the equipotential (SERT) and non-equipotential (LERT) cases are considered.

According to these two limits, expressions (2.23*a*) and (2.23*b*) are reduced, with the dispersion relation (2.22) unchanged in form. For SERT, the amplitude ratio of the initial disturbances is

$$\left(\frac{\hat{\eta}_2}{\hat{\eta}_1}\right)_1 = \frac{akRe^2H_1\Delta_3\Delta_4 + a(l^2+k^2)^2\Delta_1\Delta_4 - 4alk^3\Delta_3\left(\Delta_6 - \dfrac{1}{la}\Delta_4\right) - 2k(l^2+k^2)\Delta_3\Delta_4}{(l^2+k^2)^2\Delta_4/k - 4k^3\Delta_3}, \tag{3.6a}$$

$$\left(\frac{\hat{\eta}_1}{\hat{\eta}_2}\right)_2 = \frac{kRe^2H_2\Delta_3\Delta_4 - (l^2+k^2)^2\Delta_2\Delta_4 + 4lk^3\Delta_3\left(\Delta_5 + \dfrac{1}{l}\Delta_4\right) - 2k(l^2+k^2)\Delta_3\Delta_4}{4k^3\Delta_3 - (l^2+k^2)^2\Delta_4/k}, \tag{3.6b}$$

where H_1 is the same as (2.24*a*) and

$$H_2 = \frac{\mathrm{i}Q\omega}{k}\left(\mathrm{i}\omega L - \frac{2}{b^2-1}\right) + Eu(1+kJ) - \frac{1}{We}(1-k^2). \tag{3.7}$$

For LERT, the amplitude ratio of the initial disturbances has the same form as (2.24*a*) and (2.24*b*), but with

$$\zeta = \frac{-k\left(1+\dfrac{l^2}{k^2}\right)\dfrac{\Delta_2}{\Delta_3} + 2l\dfrac{\Delta_5}{\Delta_4} + \dfrac{Re\omega J}{k}}{\dfrac{Re\omega}{k}(\varepsilon_{r2}\kappa - J) + \dfrac{EuRe}{\omega}\left(k\dfrac{\Delta_2}{\Delta_3} - l\dfrac{\Delta_5}{\Delta_4}\right)}, \tag{3.8a}$$

$$\xi = \frac{\left(1+\dfrac{l^2}{k^2}\right)\dfrac{1}{\Delta_3} - \dfrac{2}{\Delta_4}}{\dfrac{Re\omega}{k}(\varepsilon_{r2}\kappa - J) + \dfrac{EuRe}{\omega}\left(k\dfrac{\Delta_2}{\Delta_3} - l\dfrac{\Delta_5}{\Delta_4}\right)}. \tag{3.8b}$$

Figure 6 illustrates the growth rates of the unstable modes for these two limit cases, solid curves for SERT (i.e. $\tau \to 0$) and dashed curves for LERT (i.e. $\tau \to \infty$), where several values of the electrical Euler number are considered. It can be seen from figure 6(*a*) that for the para-varicose mode only solid curves for SERT appear when the electric field exists. The difference between the two limit cases is remarkable, because for LERT the growth rate of the para-varicose mode decreases to zero when the electrical Euler number exceeds 0.01. However, for SERT the growth rate is enhanced by the electric field and the unstable region moves towards relatively short waves. On the other hand, for the para-sinuous mode as shown in figure 6(*b*), the difference between two limit cases is discernible but not significant for the range of *Eu* studied, indicating that the influence of the relative electrical relaxation time τ on the jet instability is small. This may be attributed to the large relative electrical permittivity of the outer liquid ($\varepsilon_{r2} = 80$), which makes $k\varepsilon_{r2}(\omega+\tau)\kappa$ in the denominators of (2.24*d*) and (2.24*e*) a large term, and consequently the influence of τ is weakened.

In addition, we study the influence of the relative electrical permittivity ε_{r2} on the growth rate of the para-sinuous mode. Figure 7(*a*, *b*) illustrates the results, where the electrical Euler number is fixed at 0.15 and 0.45, respectively, and the limit case

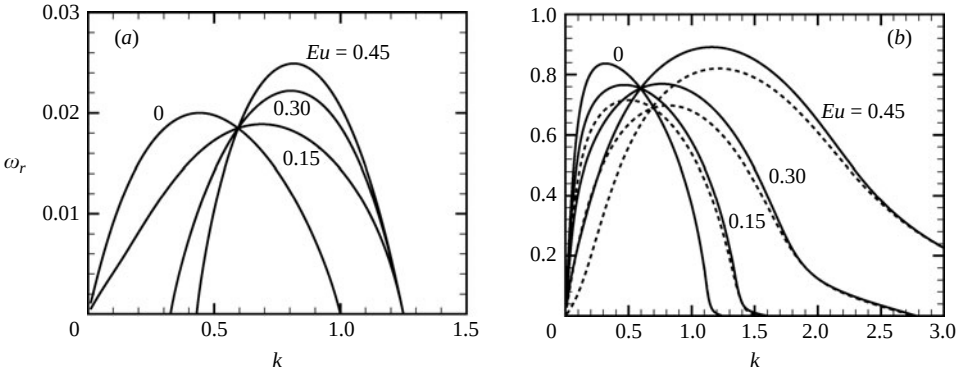

FIGURE 6. The growth rates of (*a*) the para-varicose mode and (*b*) the para-sinuous mode for the limit cases SERT (solid curves) and LERT (dashed curves) for different electrical Euler numbers.

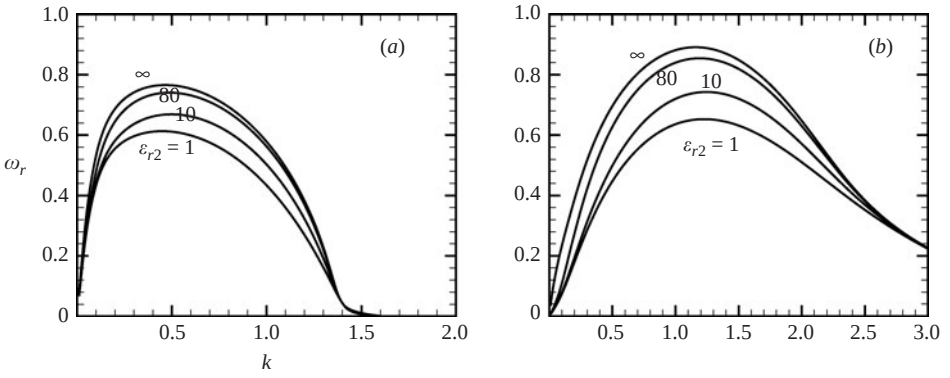

FIGURE 7. The influence of the relative electrical permittivity of the outer liquid on the growth rate of the para-sinuous mode for (*a*) $Eu = 0.15$, (*b*) $Eu = 0.45$.

$\varepsilon_{r2} \to \infty$ is also plotted. It can be seen in the figure that for both the electrical Euler numbers, the growth rate of the para-sinuous mode is enhanced with ε_{r2} increasing. When $\varepsilon_{r2} = 80$, the para-sinuous mode approaches the limit case $\varepsilon_{r2} \to \infty$ very closely. Therefore, both the limits $\varepsilon_{r2} \to \infty$ and $\tau \to \infty$ reduce the general dispersion relation (2.22) to that for the equipotential case. Moreover, it is proved that SERT may serve as an approximation for the viscous leaky dielectric model when the electrical permittivity of the outer liquid is sufficiently large.

3.3. *Effect of the electric field together with the other parameters on the jet instability*

For the inviscid coaxial jet under a radial electric field (Li *et al.* 2006), it is found that the radial electric field has a dual effect on both the para-varicose and para-sinuous modes, destabilizing them greatly when the axial wavenumber k exceeds a critical value, and stabilizing them if k is smaller than that value. In the present viscous model, the dual effect of the electric field is persistent for both the para-varicose mode and para-sinuous mode, as shown in figure 6.

It is well known that when arbitrary disturbances are applied to the jet, the perturbation wave with maximum growth rate and those close to it grow faster than the others, which become dominant in the jet breakup process. Although two unstable modes occur in the jet instability process, the para-sinuous mode is much less

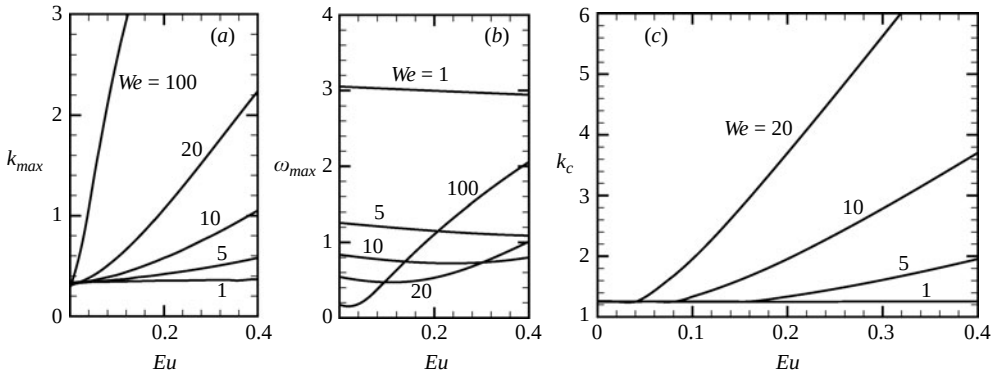

FIGURE 8. (*a*) The dominant axial wavenumber k_{max}, (*b*) the maximum growth rate ω_{max}, and (*c*) the cut-off axial wave number k_c, versus the electrical Euler number for different Weber numbers.

stable than the para-varicose one in most situations. Consequently, the most unstable wavenumber k_{max} comes from the para-sinuous mode. In figure 6(*b*), the value of k_{max} is amplified as the electrical Euler number increases, predicting that the most likely wavelength $\lambda = 2\pi R_2/k_{max}$ is diminished by the radial electric field.

It is necessary to study the effect of several important dimensionless parameters, such as the Weber number and Reynolds number, on the dominant wavenumber k_{max} and corresponding maximum growth rate ω_{max}. Figure 8(*a*, *b*) illustrates the effect of the Weber number and electrical Euler number on k_{max} and ω_{max}, respectively. The selected values of the Weber number are relatively small, since the coaxial jet is very thin and the surface tension is generally large in the experiments. It is found that the electric field influences k_{max} and ω_{max} slightly when the Weber number is relatively small ($We < 5$). However, at relatively large Weber numbers ($We > 10$), the electric field enhances k_{max} and ω_{max} distinctly. The behaviour of k_{max} and ω_{max} indicates that at small Weber numbers the jet instability is dominated primarily by the capillary force, while with the increase of *We*, the jet instability is dominated primarily by the electrical force. On the other hand, both the electrical Euler number and Weber number change the cut-off wavenumber k_c significantly, as shown in figure 8(*c*). Obviously, k_c is enlarged as *We* increases, especially at large Euler numbers. So the instability region may be extended into the first wind-induced regime, which reduces the formation of monodisperse droplets in oacxial electrospraying.

Figure 9 illustrates the effect of the Reynolds number on the dominant wavenumber k_{max} and maximum growth rate ω_{max}. In figure 9(*a*) it is apparent that the effect of the Reynolds number on k_{max} is basically small. On the other hand, the Reynolds number has a remarkable effect on the maximum growth rate, as shown in figure 9(*b*). In general, liquid viscosity stabilizes the jet significantly. Note that in figure 9(*a*) the curve corresponding to $Re = 1$ seems unusual and that in figure 9(*b*) the maximum growth rate for $Re = 1$ is very small. This reminds us that at such a low Reynolds number the non-axisymmetric modes may become comparable to or even less stable than the axisymmetric modes. In practice, in experiments most successful coaxial electrospinning, which is a typical unstable non-axisymmetric characteristic, uses highly viscous liquids. The competition between the axisymmetric and non-axisymmetric modes under an electric field is of both theoretical and practical interest, which deserves special study. Also note that for the range of the electrical

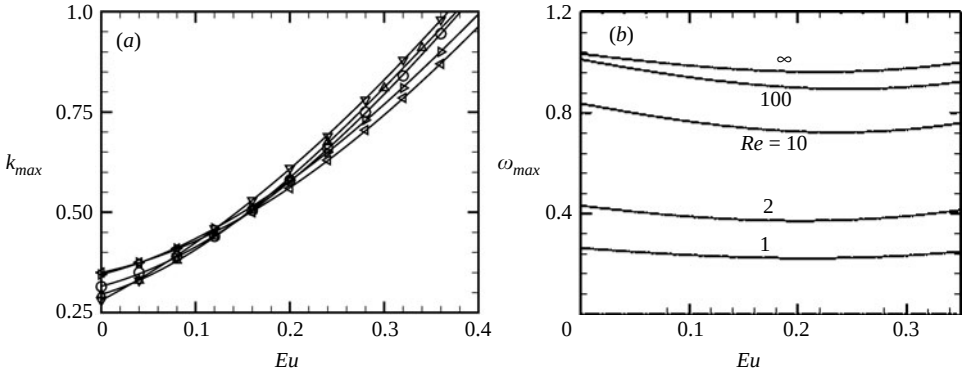

FIGURE 9. (*a*) The dominant axial wavenumber k_{max} and (*b*) the maximum growth rate ω_{max} versus the electrical Euler number for different Reynolds numbers. In (*a*): Δ, $Re = 1$; ∇, $Re = 2$; $\bigcirc$, $Re = 10$; $\triangleright$, $Re = 100$; $\triangleleft$, $Re = \infty$.

Euler number Eu considered in the figure the electric field increases k_{max} greatly but influences ω_{max} little for the Reynolds numbers studied.

3.4. *Discussion on the thin layer approximation* $a \to 1$

For coflowing jets, one extreme case is that the thickness of the outer annular liquid layer is thin. In this section, we seek relatively simple dispersion relations applicable to the thin layer coating case $a \to 1$ for case I and case II. Some details are given in Appendix C, where case I is taken as an example. The thin layer approximation ultimately results in the dispersion relation

$$\omega^2\left(QL - S\frac{I_0(k)}{I_1(k)}\right) + 2\mathrm{i}\omega\left(\frac{Q}{b^2-1} - S\Lambda\right) + \frac{1+\Gamma}{We}k(1-k^2) - Eu(1+kJ)\left(1 - \frac{\omega(1+kJ)}{\varepsilon_{r1}(\omega+\tau)\dfrac{I_1(k)}{I_0(k)} - \omega J}\right) = 0 \qquad (3.9)$$

for case I, and

$$\omega^2\frac{S}{k}\frac{I_0(k)}{I_1(k)} + \frac{2\mu_r\omega}{Re}\left(2k\frac{I_0(k)}{I_1(k)} - 1\right) + \frac{4\mu_r^2k^2}{S\,Re^2}\left(k\frac{I_0(k)}{I_1(k)} - l_1\frac{I_0(l_1)}{I_1(l_1)}\right) + \frac{\mathrm{i}Q\omega}{k}\left(\mathrm{i}\omega L - \frac{2}{b^2-1}\right) + Eu(1+kJ) - \frac{1+\Gamma}{We}(1-k^2) - \frac{SEu\left[k\omega\left(J + \dfrac{I_0(k)}{I_1(k)}\right) + \dfrac{2\mu_rk^2}{S\,Re}\left(k\dfrac{I_0(k)}{I_1(k)} - l_1\dfrac{I_0(l_1)}{I_1(l_1)}\right)\right]^2}{Sk\omega\left(\omega J - \varepsilon_{r1}(\omega+\tau)\dfrac{I_1(k)}{I_0(k)}\right) + k^2Eu\left(k\dfrac{I_0(k)}{I_1(k)} - l_1\dfrac{I_0(l_1)}{I_1(l_1)}\right)} = 0 \qquad (3.10)$$

for case II. The above expressions appear much simpler than for the coaxial jet. However, their validity needs to be evaluated. Note that under the thin layer approximation the viscosity and dynamic force of the outer liquid, as well as the electrical permittivity of the outer liquid, have no influence. Only the electrical permittivity of the inner liquid and the electrical relaxation time of the outer liquid layer play a role. Especially in the limit case $\tau \to \infty$ equations (3.9) and (3.10),

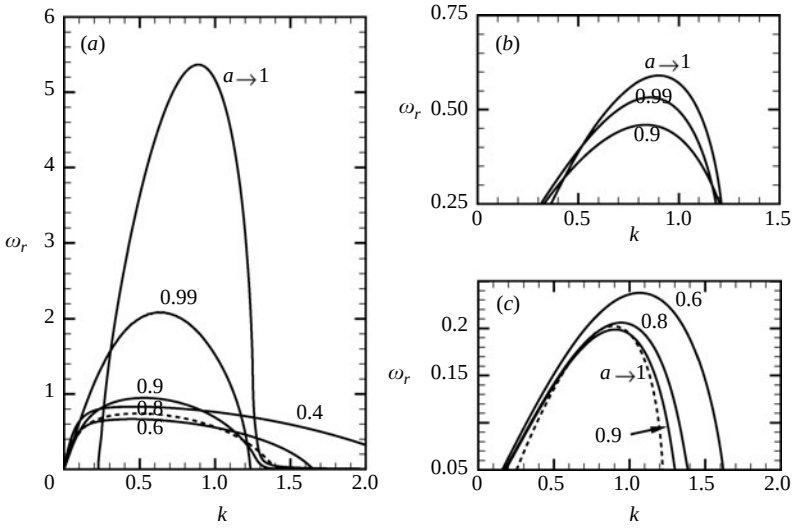

FIGURE 10. The effect of the radius ratio a on the growth rate of the para-sinuous mode for case I: (a) the reference state, (b) $S=0.1$ and (c) $S=0.84$, $\Lambda=0$. The curves for $a=0.8$ in (a) and $a\to\infty$ in (c) are dashed to make the plot clearer.

respectively, reduce to

$$\omega^2\left(QL-S\frac{I_0(k)}{I_1(k)}\right)+2\mathrm{i}\omega\left(\frac{Q}{b^2-1}-S\Lambda\right)+\frac{1+\Gamma}{We}k(1-k^2)-Eu(1+kJ)=0, \quad (3.11)$$

and

$$\omega^2\frac{S}{k}\frac{I_0(k)}{I_1(k)}+\frac{2\mu_r\omega}{Re}\left(2k\frac{I_0(k)}{I_1(k)}-1\right)+\frac{4\mu_r^2k^2}{SRe^2}\left(k\frac{I_0(k)}{I_1(k)}-l_1\frac{I_0(l_1)}{I_1(l_1)}\right)$$
$$+\frac{\mathrm{i}Q\omega}{k}\left(\mathrm{i}\omega L-\frac{2}{b^2-1}\right)+Eu(1+kJ)-\frac{1+\Gamma}{We}(1-k^2)=0. \quad (3.12)$$

The dispersion relations (3.11) and (3.12) accord with those for the single-liquid jet in the equipotential case but with double surface tension, the former for the inviscid liquid and the latter for the viscous liquid.

Figure 10 illustrates the effect of the radius ratio a on the growth rate of the para-sinuous mode for case I, where the thin layer approximation $a\to1$ is also plotted. In figure 10(a), where the other parameters are kept at reference values, the growth rate of the para-sinuous mode is sensitive to the magnitude of a as it approaches 1, and the growth rate is dramatically increased, probably owing to the relatively low density of the inner liquid and ambient air. In figure 10(b), where the density of the inner liquid is increased a little, the difference of the growth rate between case $a=0.9$ and the limit case $a\to1$ is reduced. Furthermore, when the density of the inner liquid is comparable to that of the outer liquid, as shown in figure 10(c), the thin layer approximation seems to be a good estimation. It can also be seen in the figure that the density of the inner liquid influences the growth rate of the para-sinuous mode considerably. Its effect, as well as the validity of the thin layer approximation in the other parameter regions, needs to be studied further. On the other hand, the calculation result shows that as the Reynolds number varies the para-sinuous mode always approaches the limit case as a increases. For relatively large Reynolds numbers

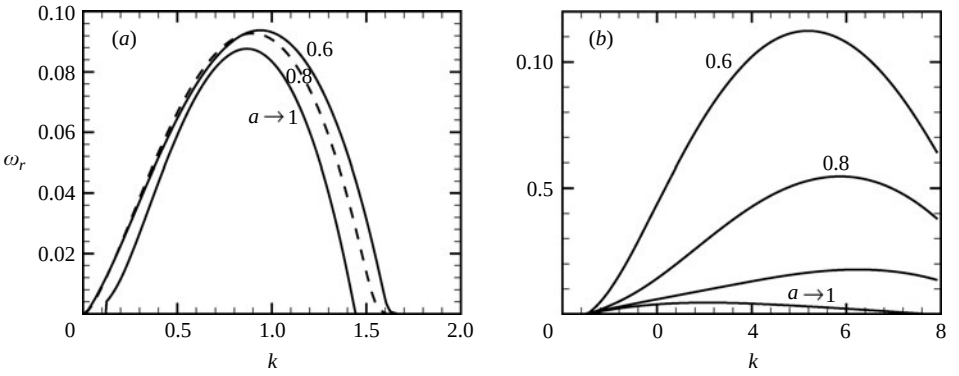

FIGURE 11. The effect of the radius ratio a on the growth rate of the para-sinuous mode for case II: (a) $Eu = 0.15$, $\mu_r = 1.0$, and (b) $Eu = 0.45$, $\mu_r = 43$. The other parameters are $Q = 0.001$, $S = 0.84$, $a = 0.8$, $b = 10$, $\Lambda = 0.2$, $Re = 10$, $We = 10$, $\Gamma = 0.23$, $\varepsilon_{r1} = 3.4$, $\varepsilon_{r2} = 80$ and $\tau = 1$. The dashed line for $a = 0.8$ in (a) is to make the plot clear.

the approach is quicker. This is easily understood by considering that in equation (3.9) viscosity is absent. Our calculation result also shows that when the radius ratio a approaches 1, the growth rate of the para-varicose mode becomes negligible. The result accords well with the theoretical prediction in Appendix C.

The effect of the radius ratio a on the growth rate of the para-sinuous mode for case II is shown in figure 11, with the thin layer approximation $a \to 1$ plotted. In figure 11(a), where the electrical Euler number and the inner liquid viscosity are relatively small, the para-sinuous mode is stabilized slightly as a approaches 1. However, in figure 11(b), where the electric Euler number and inner liquid viscosity are relatively larger, the para-sinuous mode is stabilized dramatically as a increases. For the former case, the thin layer approximation predicts the jet instability well, but for the latter, it is inaccurate.

4. Conclusions

In this paper, we study the temporal linear instability of a charged coflowing jet with two immiscible viscous liquids under a radial electric field. The analytical dimensionless dispersion relation is derived for axisymmetric disturbances and the complex eigen-frequency is solved numerically. Two different unstable modes, i.e. the para-sinuous mode and the para-varicose mode, are found in the Rayleigh regime. According to the calculation results, the para-sinuous mode is much more unstable than the para-varicose mode, and become dominant in the jet instability.

It is found that the viscosity of the outer liquid and the inner liquid, as well as the shear in the basic axial velocity, have a stabilizing effect on the jet instability, both the para-varicose mode and para-sinuous mode being considerably suppressed by them. However, the liquid viscosity and shear in the basic axial velocity have little influence on the unstable wavenumber range.

From the leaky dielectric model, two limit cases, namely the small electrical relaxation time limit (SERT) and the large electrical relaxation time limit (LERT), are obtained, based on the relative magnitude of the electrical relaxation time and the hydrodynamic time. For the para-sinuous mode, the difference between these two limits is negligible as long as the electrical permittivity of the outer liquid is sufficiently large, and in such a situation SERT can be used instead of the leaky dielectric model.

Similarly to the inviscid model, the radial electric field has a two-fold effect on the growth rate of the para-sinuous mode, stabilizing it for wavenumbers smaller than a critical value and destabilizing it when the wavenumber exceeds that value. Moreover, the dominant wavenumber and maximum growth rate, as well as the cut-off wavenumber, are generally amplified by the electric field. The Weber number has a similar effect on the dominant wavenumber and maximum growth rate.

The thin layer approximation is discussed briefly. Under the thin layer approximation, only one unstable mode, i.e. the para-sinuous mode, exists. Compared with the exact solution of the leaky dielectric model, if the viscosity of the inner liquid is neglected the thin layer approximation is more accurate when the density of the inner liquid is comparable to that of the outer liquid, but if the inner liquid viscosity is taken into account the thin layer approximation is accurate only for a relatively small electric field.

The authors are indebted to the referees for many valuable comments that helped to improve the manuscript. The work was supported by the National Natural Science Foundation of China Project No. 10572137 and the Graduate Innovation Project of USTC No. KD2005036.

Appendix A. Derivation of the dispersion relation for case I

In case I, the inner liquid and air are inviscid, with parabolic basic velocity profiles. In such a case, the radial component of the velocity satisfies the following Bessel equation (Lim & Redekopp 1998):

$$\frac{\mathrm{d}^2\hat{u}_{1,3}}{\mathrm{d}r^2} + \frac{1}{r}\frac{d\hat{u}_{1,3}}{\mathrm{d}r} - \left(k^2 + \frac{1}{r^2}\right)\hat{u}_{1,3} = 0, \tag{A 1}$$

where the 'hats' stand for the initial perturbation amplitudes. The solutions of (A 1) are the linear combination of the modified Bessel functions. Their coefficients are determined by using the boundary conditions (2.3) and (2.6)–(2.8). Suppose that the cylindrical coordinate system (r, θ, z) is moving with velocity U_2, then the solutions are

$$\hat{u}_1 = \omega\hat{\eta}_1\frac{I_1(kr)}{I_1(ka)}, \quad \hat{u}_3 = \omega\hat{\eta}_2\frac{I_1(kr)K_1(kb) - K_1(kr)I_1(kb)}{I_1(k)K_1(kb) - K_1(k)I_1(kb)}. \tag{A 2}$$

The axial velocity and pressure can be obtained using equations (2.1) and (2.2).

As the outer liquid is viscous, we decompose the velocity perturbation into two terms (González *et al.* 2003; López-Herrera *et al.* 2005), i.e. $\boldsymbol{u}_2 = \boldsymbol{u}_p + \boldsymbol{u}_v$, where $\boldsymbol{u}_p$ and $\boldsymbol{u}_v$ satisfy the following linearized equations:

$$\nabla\cdot\boldsymbol{u}_p = 0, \quad \frac{\partial\boldsymbol{u}_p}{\partial t} = -\nabla p_2, \quad \nabla\cdot\boldsymbol{u}_v = 0, \quad \frac{\partial\boldsymbol{u}_v}{\partial t} = \frac{1}{Re}\nabla^2\boldsymbol{u}_v. \tag{A 3}$$

For $\boldsymbol{u}_p$, a potential function ϕ_2 ($\boldsymbol{u}_p = \nabla\phi_2$) is introduced, which satisfies the Laplace equation $\nabla^2\phi_2 = 0$. Therefore, the amplitude $\hat{\phi}_2$ satisfies the modified Bessel equation

$$\frac{\mathrm{d}^2\hat{\phi}_2}{\mathrm{d}r^2} + \frac{1}{r}\frac{\mathrm{d}\hat{\phi}_2}{\mathrm{d}r} - k^2\hat{\phi}_2 = 0. \tag{A 4}$$

The solution is $\hat{\phi}_2 = A_1 I_0(kr) + A_2 K_0(kr)$, where A_1 and A_2 are coefficients to be determined by boundary conditions. The amplitudes of the radial and axial velocity components and the pressure can also be obtained.

For the viscous part, the radial momentum equation yields

$$\frac{\mathrm{d}^2\hat{u}_v}{\mathrm{d}r^2} + \frac{1}{r}\frac{\mathrm{d}\hat{u}_v}{\mathrm{d}r} - \left(k^2 + Re\omega + \frac{1}{r^2}\right)\hat{u}_v = 0. \tag{A 5}$$

The solution is $\hat{u}_v = A_3 I_1(lr) + A_4 K_1(lr)$, where A_3 and A_4 are coefficients to be determined, and $l = \sqrt{k^2 + Re\omega}$. Then the continuity equation gives the solution of the axial velocity component, $\hat{w}_v = \mathrm{i}l(A_3 I_0(lr) - A_4 K_0(lr))/k$.

For the electric field, the perturbations of the electrical potentials, ψ_i, $i = 1, 2, 3$, also satisfy the Laplace equation (2.11). Further, their perturbation amplitudes $\hat{\psi}_i$, also satisfy the modified Bessel equation (A 4). Consequently their solutions are the linear combinations of two modified Bessel functions $I_0(kr)$ and $K_0(kr)$, which gives five coefficients A_5–A_9 to be determined.

For the present problem, there are in all twelve unknown quantities: A_1–A_9, $\hat{\eta}_1$, $\hat{\eta}_2$ and $\hat{q}_s$ (the perturbation amplitude of the surface charge density). On the other hand, the boundary conditions (2.7)–(2.8) and (2.12)–(2.17) provide twelve equations to solve the unknown. These equations set up a homogeneous linear system. The system has non-trivial solutions only if the determinant of its coefficient matrix is null, which provides the dispersion relation we need. However, considering the size of the coefficient matrix, it is hard to obtain an explicit expression for the dispersion relation in such a way. Therefore, we choose to solve the equations step by step as outlined in the following, aiming to obtain the dispersion relation in a more compact form.

For the outer liquid, according to the continuity equation,

$$\hat{w}_2 = \frac{\mathrm{i}}{k}\left(\frac{\mathrm{d}\hat{u}_2}{\mathrm{d}r} + \frac{\hat{u}_2}{r}\right). \tag{A 6}$$

Differentiating the above equation with respect to $r$and using the momentum equation in the radial direction, we have

$$\frac{\mathrm{d}\hat{w}_2}{\mathrm{d}r} = \frac{\mathrm{i}}{k}\left(l^2\hat{u}_2 + Re\frac{\mathrm{d}\hat{p}_2}{\mathrm{d}r}\right). \tag{A 7}$$

Then using the linearized kinematic boundary conditions at the interfaces, we obtain

$$\left.\frac{\mathrm{d}\hat{w}_2}{\mathrm{d}r}\right|_{r=a+\eta_1} = \frac{\mathrm{i}\omega}{k}[l^2\hat{\eta}_1 - Rek(A_1 I_1(ka) - A_2 K_1(ka))], \tag{A 8a}$$

$$\left.\frac{\mathrm{d}\hat{w}_2}{\mathrm{d}r}\right|_{r=1+\eta_2} = \frac{\mathrm{i}\omega}{k}[l^2\hat{\eta}_2 - Rek(A_1 I_1(k) - A_2 K_1(k))]. \tag{A 8b}$$

Substituting the corresponding solutions into the linearized kinematic boundary conditions and the tangential dynamic boundary conditions, we obtain the expressions for $A_1 - A_4$. The process and the expressions are omitted for brevity. On the other hand, substituting the corresponding solutions into the electric field boundary conditions, we can obtain $A_5 - A_9$. Finally, substituting the expressions for the corresponding quantities into the linearized normal dynamic boundary conditions, (2.23a) and (2.23b) are obtained, together with the dispersion relation (2.22).

Appendix B. Derivation of the dispersion relation for case II

In case II, the dispersion relation is also written in the form of equation (2.22), but with the amplitude ratio of the interface perturbation:

$$\begin{aligned}\left(\frac{\hat{\eta}_2}{\hat{\eta}_1}\right)_1 = &\left[\frac{\Delta_4}{a}\left(\frac{\Pi}{\mathrm{H}}+\omega\right)\left(\frac{EuRe\zeta}{\omega}+1+\frac{l_2^2}{k^2}\right)-\frac{\Delta_3}{a}\frac{\Pi}{\mathrm{H}}\left(\frac{EuRe\zeta}{\omega}+2\right)\right]^{-1}\\ &\times\left[k\Delta_1\Delta_4\left(\frac{\Pi}{\mathrm{H}}+\omega\right)\left(1+\frac{l_2^2}{k^2}-\mu_r\left(1+\frac{l_1^2}{k^2}\right)\right)\right.\\ &-l_2\Delta_3\Delta_6\frac{\Pi}{\mathrm{H}}\left(2-\mu_r\left(1+\frac{l_1^2}{k^2}\right)\right)\\ &+\omega\Delta_3\Delta_4\left(2(1-\mu_r)\left(\Theta-\frac{1}{a}\right)-\frac{Re\Theta}{k^2}\frac{\Pi}{\mathrm{H}}\right)\\ &\left.+\frac{\Gamma}{We\,a^2}(1-(ka)^2)Re\Delta_3\Delta_4+\frac{EuRe\xi}{\omega}\frac{1}{a}\left(\frac{\Pi}{\mathrm{H}}\Delta_3-\left(\frac{\Pi}{\mathrm{H}}+\omega\right)\Delta_4\right)\right], \quad (\mathrm{B}\,1a)\end{aligned}$$

$$\begin{aligned}\left(\frac{\hat{\eta}_1}{\hat{\eta}_2}\right)_2 = &\left[\Delta_4\left(1+\frac{l_2^2}{k^2}-\mu_r\left(1+\frac{l_1^2}{k^2}\right)\right)\left(-(l_2^2+k^2)+\frac{Sk^2\Xi\Delta_1}{\mathrm{H}\Delta_3\Delta_4}\right)\right.\\ &+\Delta_3\left(2-\mu_r\left(1+\frac{l_1^2}{k^2}\right)\right)\left(2k^2-\frac{Skl_2\Xi\Delta_6}{\mathrm{H}\Delta_3\Delta_4}\right)\\ &-\frac{SRe\omega\Theta\Xi}{k\mathrm{H}}-Re^2\Delta_3\Delta_4Euk\xi J+\frac{EuRe\xi}{\omega}\left(\frac{Sk\Xi}{a\mathrm{H}}\left(\frac{1}{\Delta_4}-\frac{1}{\Delta_3}\right)\right.\\ &\left.\left.+k^3\Delta_2\Delta_4\left(1+\frac{l_2^2}{k^2}\right)-2l_2k^2\Delta_3\Delta_5\right)\right]^{-1}\left[-\frac{Sk\Xi^2}{a\mathrm{H}\Delta_3\Delta_4}+Re^2H_2\Delta_3\Delta_4\right.\\ &-k\Delta_4\left(\left(l_2^2+k^2\right)\Delta_2+2k\Delta_3\right)\left(\frac{EuRe\zeta}{\omega}+1+\frac{l_2^2}{k^2}\right)+2l_2k^2\Delta_3\\ &\left.\times\left(\Delta_5+\frac{1}{l_2}\Delta_4\right)\left(\frac{EuRe\zeta}{\omega}+2\right)-\frac{EuRe\zeta}{\omega}\frac{Sk\Xi}{a\mathrm{H}}\left(\frac{1}{\Delta_4}-\frac{1}{\Delta_3}\right)\right], \quad (\mathrm{B}\,1b)\end{aligned}$$

where

$$\begin{aligned}&l_1=\sqrt{k^2+Re\omega S/\mu_r}, \quad l_2=\sqrt{k^2+Re\omega},\\ &\Pi=S\omega\left(\frac{\Delta_1}{\Delta_3}-\frac{I_0(ka)}{I_1(ka)}\right)+\frac{2(1-\mu_r)k^2}{Re}\left(\frac{I_0(ka)}{I_1(ka)}-\frac{\Theta}{k}\right),\\ &\mathrm{H}=\frac{I_0(ka)}{I_1(ka)}-\frac{\Theta}{k}-S\left(\frac{\Delta_1}{\Delta_3}-\frac{l_2}{k}\frac{\Delta_6}{\Delta_4}\right),\\ &\Theta=l_1\frac{I_0(l_1a)}{I_1(l_1a)}, \quad \Xi=2\Delta_3-\Delta_4\left(1+\frac{l_2^2}{k^2}\right)\end{aligned}$$

$$\begin{aligned}\zeta = &\left[\varepsilon_{r2}(\omega+\tau)\kappa-\omega J+\frac{Eu}{\omega}\left(\frac{S}{a\mathrm{H}}\left(\frac{1}{\Delta_3}-\frac{1}{\Delta_4}\right)^2+k\left(k\frac{\Delta_2}{\Delta_3}-l_2\frac{\Delta_5}{\Delta_4}\right)\right)\right]^{-1}\\ &\times\left[\omega J-\frac{k^2\Delta_2}{Re\,\Delta_3}\left(1+\frac{l_2^2}{k^2}\right)+\frac{2l_2k\Delta_5}{Re\,\Delta_4}-\frac{S}{Re\,a\mathrm{H}}\left(\frac{1}{\Delta_3}-\frac{1}{\Delta_4}\right)\left(\frac{1}{\Delta_3}\left(1+\frac{l_2^2}{k^2}\right)-\frac{2}{\Delta_4}\right)\right],\end{aligned}$$

$$\xi = \left[\varepsilon_{r2}(\omega+\tau)\kappa - \omega J + \frac{Eu}{\omega}\left(\frac{S}{a\mathrm{H}}\left(\frac{1}{\Delta_3}-\frac{1}{\Delta_4}\right)^2 + k\left(k\frac{\Delta_2}{\Delta_3} - l_2\frac{\Delta_5}{\Delta_4}\right)\right)\right]^{-1}$$
$$\times \left[\frac{k}{Re\,\Delta_3}\left(1+\frac{l_2^2}{k^2}-\mu_r\left(1+\frac{l_1^2}{k^2}\right)\right)\left(1+\frac{S\Delta_1}{\mathrm{H}}\left(\frac{1}{\Delta_3}-\frac{1}{\Delta_4}\right)\right)\right.$$
$$\left. - \frac{k}{Re\,\Delta_4}\left(2-\mu_r\left(1+\frac{l_1^2}{k^2}\right)\right)\left(1+\frac{l_2 S\Delta_6}{k\mathrm{H}}\left(\frac{1}{\Delta_3}-\frac{1}{\Delta_4}\right)\right) - \frac{S\omega\Theta}{k^2\mathrm{H}}\left(\frac{1}{\Delta_3}-\frac{1}{\Delta_4}\right)\right].$$

and the relative viscosity of the inner liquid $\mu_r = \mu_1/\mu_2$. Note that κ, H_2 and the other symbols are the same as in case I. It is shown that the dispersion relation for case II reduces to that for case I as long as the viscosity of the inner liquid is neglected (i.e. $\mu_r = 0$). The inner liquid viscosity makes the problem much more complicated.

Appendix C. Derivation of the thin layer approximation $a \to 1$

In the instability analysis of an annular viscous liquid jet, the thin sheet approximation is usually derived (Meyer & Weihs 1987; Shen & Li 1996; Chen *et al.* 2003). If the inner and outer radii of the annular jet are supposed to approach infinity with the thickness of the liquid layer constant, a plane liquid sheet is obtained, as in Meyer & Weihs (1987) and Shen & Li (1996). But in this paper, we follow the approach similar to Chen *et al.* (2003), expanding the dispersion relation under the thin layer limit. The derivation process is outlined below, taking case I as an example.

Define a quantity $\delta = 1-a$. We expand the dispersion relation (2.22) under the thin layer approximation $\delta \ll 1$. First, the expansions of $\Delta_0 - \Delta_6$ are

$$\Delta_0 = -\delta - \frac{\delta^2}{2} + O(\delta^3), \quad \Delta_1 = \frac{1}{k} + \frac{k\delta^2}{2} + O(\delta^3), \tag{C 1a}$$

$$\Delta_2 = \frac{1}{k} + \frac{\delta}{k} + \frac{k\delta^2}{2}\left(1+\frac{2}{k^2}\right) + O(\delta^3), \quad \Delta_3 = -\delta - \frac{\delta^2}{2} - \frac{k^2\delta^3}{6}\left(1+\frac{3}{k^2}\right) + O(\delta^4), \tag{C 1b}$$

$$\Delta_4 = -\delta - \frac{\delta^2}{2} - \frac{l^2\delta^3}{6}\left(1+\frac{3}{l^2}\right) + O(\delta^4), \quad \Delta_5 = \frac{1}{l} + \frac{\delta}{l} + \frac{l\delta^2}{2}\left(1+\frac{2}{l^2}\right) + O(\delta^3), \tag{C 1c}$$

$$\Delta_6 = \frac{1}{l} + \frac{l\delta^2}{2} + O(\delta^3). \tag{C 1d}$$

Then, the expansions of κ, ζ and ξ are

$$\kappa = \frac{\varepsilon_{r1}}{\varepsilon_{r2}}\frac{I_1(k)}{I_0(k)} + k\left(1-\frac{\varepsilon_{r1}}{\varepsilon_{r2}}\right)\left[1+\frac{\varepsilon_{r1}}{\varepsilon_{r2}}\left(\frac{I_1(k)}{I_0(k)}\right)^2\right]\delta + O(\delta^2), \tag{C 2a}$$

$$\zeta = \frac{\dfrac{k}{Re}\left(\dfrac{1}{\delta}+\dfrac{1}{2}\right)\left(\dfrac{l^2}{k^2}-1\right) + \omega J + \dfrac{k}{Re}\left(\dfrac{l^2}{k^2}-1\right)\left(\dfrac{1}{4}-\dfrac{k^2}{3}\right)\delta + O(\delta^2)}{\varepsilon_{r1}(\omega+\tau)\dfrac{I_1(k)}{I_0(k)} - \omega J + \left(\varepsilon_{r2}(\omega+\tau)\kappa_{O(\delta)} - \dfrac{EuRek}{6}\right)\delta + O(\delta^2)}, \tag{C 2b}$$

$$\xi = \frac{\dfrac{k}{Re}\left(-\dfrac{1}{\delta}+\dfrac{1}{2}\right)\left(\dfrac{l^2}{k^2}-1\right) + \dfrac{k}{Re}\left(\dfrac{l^2}{k^2}-1\right)\left(\dfrac{1}{4}-\dfrac{k^2}{6}\right)\delta + O(\delta^2)}{\varepsilon_{r1}(\omega+\tau)\dfrac{I_1(k)}{I_0(k)} - \omega J + \left(\varepsilon_{r2}(\omega+\tau)\kappa_{O(\delta)} - \dfrac{EuRek}{6}\right)\delta + O(\delta^2)}, \tag{C 2c}$$

where $\kappa_{O(\delta)}$ represents a coefficient of $O(\delta)$ in the expansion of κ. Now we write the coefficients of the interface perturbation amplitudes $\hat{\eta}_1$ and $\hat{\eta}_2$ individually for each order, i.e.
for $O(1)$,

$$(\hat{\eta}_1)_1: \quad (l^2-k^2)\frac{EuRe\zeta_{O(1/\delta)}}{\omega}, \quad (\hat{\eta}_2)_1: \quad (k^2-l^2)\frac{EuRe\xi_{O(1/\delta)}}{\omega},$$
$$(\hat{\eta}_1)_2: \quad (k^2-l^2)\frac{EuRe\zeta_{O(1/\delta)}}{\omega}, \quad (\hat{\eta}_2)_2: \quad (l^2-k^2)\frac{EuRe\xi_{O(1/\delta)}}{\omega};$$

for $O(\delta)$,

$$\begin{aligned}
(\hat{\eta}_1)_1: \quad & Re^2 EukJ\zeta_{O(1/\delta)} + (l^2-k^2)\frac{EuRe\zeta_{O(1)}}{\omega} + \frac{(l^2+k^2)^2}{k^2} \\
& -4k^2 + \frac{3}{2}(l^2-k^2)\frac{EuRe\zeta_{O(1/\delta)}}{\omega}, \\
(\hat{\eta}_2)_1: \quad & -Re^2 EukJ\xi_{O(1/\delta)} + (k^2-l^2)\frac{EuRe\xi_{O(1)}}{\omega} + \frac{(l^2+k^2)^2}{k^2} \\
& -4k^2 + \frac{3}{2}(k^2-l^2)\frac{EuRe\xi_{O(1/\delta)}}{\omega}, \\
(\hat{\eta}_1)_2: \quad & (k^2-l^2)\frac{EuRe\zeta_{O(1)}}{\omega} - \frac{(l^2+k^2)^2}{k^2} + 4k^2 + \frac{1}{2}(k^2-l^2)\frac{EuRe\zeta_{O(1/\delta)}}{\omega}, \\
(\hat{\eta}_2)_2: \quad & (l^2-k^2)\frac{EuRe\xi_{O(1)}}{\omega} - \frac{(l^2+k^2)^2}{k^2} + 4k^2 + \frac{1}{2}(l^2-k^2)\frac{EuRe\xi_{O(1/\delta)}}{\omega};
\end{aligned}$$

for $O(\delta^2)$,

$$\begin{aligned}
(\hat{\eta}_1)_1: \quad & Re^2(H_2)_{O(1)} + \left(\frac{(l^2-k^2)^2}{6} + 2(l^2-k^2)\right)\frac{EuRe\zeta_{O(1/\delta)}}{\omega} + \frac{3}{2}(l^2-k^2)\frac{EuRe\zeta_{O(1)}}{\omega} \\
& + (l^2-k^2)\frac{EuRe\zeta_{O(\delta)}}{\omega} + Re^2 EukJ\zeta_{O(1/\delta)} + \frac{3}{2}\frac{l^4-k^4}{k^2} + l^2 - k^2, \\
(\hat{\eta}_2)_1: \quad & -Re^2 EukJ\left(\xi_{O(1/\delta)} + \zeta_{O(1)}\right) - \left(\frac{(l^2-k^2)^2}{6} + 2(l^2-k^2)\right)\frac{EuRe\xi_{O(1/\delta)}}{\omega} \\
& + \frac{3}{2}(k^2-l^2)\frac{EuRe\xi_{O(1)}}{\omega} + (k^2-l^2)\frac{EuRe\xi_{O(\delta)}}{\omega} + \frac{1}{2}\left(\frac{(l^2+k^2)^2}{k^2} - 4k^2\right), \\
(\hat{\eta}_1)_2: \quad & \left(-(l^2+k^2)\left(\frac{l^2}{6}+\frac{1}{2}\right) + 2k^2\left(\frac{k^2}{6}+\frac{1}{2}\right)\right)\frac{EuRe\zeta_{O(1/\delta)}}{\omega} \\
& + \frac{k^2-l^2}{2}\frac{EuRe\zeta_{O(1)}}{\omega} + (k^2-l^2)\frac{EuRe\zeta_{O(\delta)}}{\omega} - \frac{(l^2+k^2)^2}{2k^2} + 2k^2, \\
(\hat{\eta}_2)_2: \quad & Re^2(H_1)_{O(1)} + \left((l^2+k^2)\left(\frac{l^2}{6}+\frac{1}{2}\right) - 2k^2\left(\frac{k^2}{6}+\frac{1}{2}\right)\right)\frac{EuRe\xi_{O(1/\delta)}}{\omega} \\
& + \frac{l^2-k^2}{2}\frac{EuRe\xi_{O(1)}}{\omega} + (l^2-k^2)\frac{EuRe\xi_{O(\delta)}}{\omega} + \frac{(l^2+k^2)^2}{2k^2} - 2k^2.
\end{aligned}$$

For the first order $O(1)$, $(\hat{\eta}_2/\hat{\eta}_1)_1 = (\hat{\eta}_1/\hat{\eta}_2)_2 \approx 1$, indicating that under the thin layer approximation the amplitudes of the perturbations at the inner and outer interfaces are nearly equal. Moreover, the difference of the phase angle is nearly 0°. That is, in such a case there exists only one unstable mode close to the sinuous mode.

Substituting the above expansions into the dispersion relation, it is found that for $O(1)$ and $O(\delta)$ the dispersion relation is inherently satisfied. Therefore, the dispersion relation for the thin layer approximation is given by $O(\delta^2)$. The process of simplification is straightforward and is omitted for brevity. Ultimately the dispersion relation in the form of equation (3.9) is obtained.

REFERENCES

Artana, G., Romat, H. & Touchard, G. 1998 Theoretical analysis of linear stability of electrified jets flowing at high velocity inside a coaxial electrode. *J. Electrost.* **43**, 830–100.

Chandrasekhar, S. 1961 *Hydrodynamic and Hydromagnetic Stability*. Oxford University Press.

Chen, F., Tsaur, J.-Y., Durst, F. & Das, S. K. 2003 On the axisymmetry of annular jet instabilities. *J. Fluid Mech.* **488**, 355–367.

Chen, J. N. & Lin, S. P. 2002 Instability of an annular jet surrounded by a viscous gas in a pipe. *J. Fluid Mech.* **450**, 235–258.

Chen, X. P., Jia, L. B., Yin, X. Z., Cheng, J. S. & Lu, J. 2005 Spraying modes in coaxial jet electrospray with outer driving liquid. *Phys. Fluids* **17**, 032101.

Elhefnawy, A. R. F., Agoor, B. M. H. & Elcoot, A. E. K. 2001 Nonlinear electrohydrodynamic stability of a finitely conducting jet under an axial electric field. *Physica* A **297**, 368–388.

Elhefnawy, A. R. F., Moatimid, G. M. & Elcoot, A. E. K. 2004 Nonlinear electrohydrodynamic instability of a finitely conducting cylinder: Effect of interfacial surface charges. *Z. Angew. Math. Phys.* **55**, 63–91.

García, F. J., González, H., Ramos, A. & Castellanos, A. 1997 Stability of insulating viscous jets under axial electric fields. *J. Electrost.* **40&41**, 161–166.

González, H., García, F. J. & Castellanos, A. 2003 Stability analysis of conducting jets under ac radial electric fields for arbitrary viscosity. *Phys. Fluids* **15**, 395–407.

Higuera, F. J. 2007 Stationary coaxial electrified jet of a dielectric liquid surrounded by a conductive liquid. *Phys. Fluids* **19**, 012102.

Huebner, A. L. & Chu, H. N. 1971 Instability and breakup of charged liquid jets. *J. Fluid Mech.* **49**, 361–372.

Li, F., Yin, X. Y. & Yin, X. Z. 2005 Linear instability analysis of an electrified coaxial jet. *Phys. Fluids* **17**, 077104.

Li, F., Yin, X. Y. & Yin, X. Z. 2006 Instability analysis of a coaxial jet under a radial electric field in the nonequipotential case. *Phys. Fluids* **18**, 037101.

Lim, D. W. & Redekopp, L. G. 1998 Absolute instability conditions for variable density, swirling jet flows. *Eur. J. Mech.* B/*Fluids* **17**, 165–185.

López-herrera, J. M., Barrero, A., López, A., Loscertales, I. G. & Márquez, M. 2003 Coaxial jets generated from electrified Taylor cones. Scaling laws. *J. Aerosol Sci.* **34**, 535–552.

López-herrera, J. M. & Gañán-calvo, A. M. 2004 A note on charged capillary jet breakup of conducting liquids: experimental validation of a viscous one-dimensional model. *J. Fluid Mech.* **501**, 303–326.

López-herrera, J. M., Gañán-calvo, A. M. & Perez-saborid, M. 1999 One-dimensional simulation of the breakup of capillary jets of conducting liquids. Application to E.H.D. spraying. *J. Aerosol Sci.* **30**, 895–912.

López-herrera, J. M., Riesco-chueca, P. & Gañán-calvo, A. M. 2005 Linear stability analysis of axisymmetric perturbations in imperfectly conducting liquid jets. *Phys. Fluids* **17**, 034106.

Loscertales, I. G., Barrero, A., Guerrero, I., Cortijo, R., Márquez, M. & Gañán-calvo, A. M. 2002 Micro/nano encapsulation via electrified coaxial liquid jets. *Science* **95**, 1695–1698.

Marin, A. G., Loscertales, I. G., Marquez, M. & Barrero, A. 2007 Simple and double emulsions via coaxial jet electrosprays. *Phys. Rev. Lett.* **98**, 014502.

Melcher, J. R. & Taylor, G. I. 1969 Electrohydrodynamics: a review of the role of interfacial shear stresses. *Annu. Rev. Fluid Mech.* **1**, 111–146.

Mestel, A. J. 1994 Electrohydrodynamic stability of a slightly viscous jet. *J. Fluid Mech.* **274**, 93–113.

Mestel, A. J. 1996 Electrohydrodynamic stability of a highly viscous jet. *J. Fluid Mech.* **312**, 311–326.

Meyer, J. & Weihs, D. 1987 Capillary instability of an annular liquid jet. *J. Fluid Mech.* **179**, 531–545.

Moatimid, G. M. 2003 Non-linear electrorheological instability of two streaming cylindrical fluids. *J. Phys.* A*: Math. Gen.* **36**, 11343–11365.

Saville, D. A. 1971 Electrohydrodynamic stability: effects of charge relaxation at the interface of a liquid jet. *J. Fluid Mech.* **48**, 815–827.

Saville, D. A. 1997 Electrohydrodynamics: the Taylor-Melcher leaky dielectric model. *Annu. Rev. Fluid Mech.* **29**, 27–64.

Shen, J. & Li, X. 1996 Instability of an annular viscous liquid jet. *Acta Mech.* **114**, 167–183.

Son, P. H. & Ohba, K. 1998 Theoretical and experimental investigations on instability of an electrically charged liquid jet. *Intl J. Multiphase Flow* **24**, 605–615.

Turnbull, R. J. 1992 On the instability of an electrostatically sprayed liquid jet. *IEEE Trans. Ind. Appl.* **28**, 1432–1438.

Turnbull, R. J. 1996 Finite conductivity effects on electrostatically sprayed liquid jets. *IEEE Trans. Ind. Appl.* **32**, 837–843.

Zakaria, K. 2000 Nonlinear instability of a liquid jet in the presence of a uniform electric field. *Fluid Dyn. Res.* **26**, 405–420.